The tensile strength of hydrothermally altered volcanic rocks

Michael Heap, Claire Harnett, Fabian Wadsworth, H. Albert Gilg, Lucille Carbillet, Marina Rosas-Carbajal, Jean-Christophe Komorowski, Patrick Baud, Valentin Troll, Frances Deegan, et al.

The tensile strength of hydrothermally altered volcanic rocks

Michael J. Heap[1,2]*, Claire E. Harnett[3], Fabian B. Wadsworth[4], H. Albert Gilg[5], Lucille Carbillet[1], Marina Rosas-Carbajal[6], Jean-Christophe Komorowski[6], Patrick Baud[1], Valentin R. Troll[7], Frances M. Deegan[7], Eoghan P. Holohan[3], and Roberto Moretti[5,8]

[1]Université de Strasbourg, CNRS, Institut Terre et Environnement de Strasbourg, UMR 7063, 5 rue Descartes, Strasbourg F-67084, France

[2]Institut Universitaire de France (IUF), Paris, France

[3]UCD School of Earth Sciences, University College Dublin, Dublin, Ireland

[4]Earth Science, Durham University, Science Labs, Durham, DL1 3LE, United Kingdom

[5]Department of Civil, Geo and Environmental Engineering, Technical University of Munich, Arcisstrasse 21, 80333 Munich, Germany

[6]Université de Paris, Institut de Physique du Globe de Paris, CNRS UMR 7154, F-75005 Paris, France

[7]Department of Earth Science, Natural Resources and Sustainable Development (NRHU), Uppsala University, Villavägen 16, SE-752 36 Uppsala, Sweden

[8]Observatoire Volcanologique et Sismologique de Guadeloupe, Institut de Physique du Globe de Paris, F-97113 Gourbeyre, France

*Corresponding author: Michael Heap (heap@unistra.fr)

Abstract

The tensile strength of volcanic rocks is an important parameter for understanding and modelling a wide range of volcanic processes, and in the development of strategies designed to

optimise energy production in volcanic geothermal reservoirs. However, despite the near-ubiquity of hydrothermal alteration at volcanic and geothermal systems, values of tensile strength for hydrothermally altered volcanic rocks are sparse. Here, we present an experimental study in which we measured the tensile strength of variably altered volcanic rocks. The alteration of these rocks, quantified as the weight percentage of secondary (alteration) minerals, varied from 6 to 62.8 wt%. Our data show that tensile strength decreases as a function of porosity, in agreement with previous studies, and as a function of alteration. We fit existing theoretical constitutive models to our data so that tensile strength can be estimated for a given porosity, and we provide a transformation of these models such that they are a function of alteration. However, because porosity and alteration influence each other, it is challenging to untangle their individual contributions to the measured reduction in tensile strength. Our new data and previously published data suggest that porosity exerts a first-order role on the tensile strength of volcanic rocks. Based on our data and observations, we also suggest that (1) alteration likely decreases tensile strength if associated with mineral dissolution, weak secondary minerals (such as clays), and an increase in microstructural heterogeneity and (2) alteration likely increases tensile strength if associated with pore- and crack-filling mineral precipitation. Therefore, we conclude that both alteration intensity and alteration type likely influence tensile strength. To highlight the implications of our findings, we provide discrete element method modelling which shows that, following the pressurisation of a dyke, the damage within weak hydrothermally altered host-rock is greater and more widespread than for strong hydrothermally altered host-rock. Because the rocks in volcanic and geothermal settings are likely to be altered, our results suggest that future modelling should consider the tensile strength of hydrothermally altered volcanic rocks.

Keywords: La Soufrière de Guadeloupe; Merapi; Chaos Crags; porosity; alteration

Highlights:

- Tensile strength decreases as a function of porosity and alteration.
- Constitutive models provide tensile strength estimates for a given porosity or alteration.
- Alteration intensity and alteration type likely influence tensile strength.
- Numerical models show that alteration influences the damage surrounding a dyke.
- Volcano and geothermal modelling should consider the tensile strength of altered rocks.

1 Introduction

Hot hydrothermal fluids within a volcanic system can permanently change the rocks through which they pass, both physically and chemically (Browne, 1978). Hydrothermal alteration is thought to compromise the stability of a volcanic dome or flank, increasing the likelihood of potentially devastating collapse hazards (Day, 1996; van Wyk de Vries et al., 2000; Reid et al., 2001; Voight et al., 2002; Reid, 2004; Cecchi et al., 2004; Ball et al., 2015, Rosas-Carbajal et al., 2016; Ball et al., 2018; Mordensky et al., 2019; Heap et al., 2021a, b; Harnett and Heap, 2021; Darmawan et al., 2022). Indeed, hydrothermal alteration is prominent in both the matrix and coherent blocks within debris avalanche deposits resulting from partial edifice collapse (e.g., Salaün et al., 2011). Alteration is also considered to inhibit the outgassing of magmatic volatiles through the dome or conduit and/or restrict fluid movement, promoting erratic explosive behaviour (Boudon et al., 1998; Edmonds et al., 2003; Montanaro et al., 2016; Mayer et al., 2017; de Moor et al., 2019; Heap et al., 2019; Kennedy et al., 2020; Mick et al., 2021; Kanakiya et al., 2021).

Despite the importance and common presence of hydrothermal alteration at volcanic systems, few laboratory studies have sought to better understand the influence of hydrothermal alteration on the physical and mechanical properties of volcanic rocks. The need for more

experimental studies is further emphasised by the seemingly contradictory influence of alteration on the physical and mechanical properties of volcanic rocks. For example, experimental studies have shown that hydrothermal alteration can increase (Marmoni et al., 2017; Heap et al., 2020, 2021b) or decrease (del Potro and Hürlimann, 2009; Frolova et al., 2014; Wyering et al., 2014; Mayer et al., 2016; Farquharson et al., 2019; Heap et al., 2021a) the strength, and increase (Mayer et al., 2016; Farquharson et al., 2019) or decrease (Heap et al., 2017, 2019, 2020; Kennedy et al., 2020; Kanakiya et al., 2021) the permeability of volcanic rocks. It was also recently shown that hydrothermal alteration can increase or decrease the thermal properties (thermal conductivity, thermal diffusivity, specific heat capacity) of volcanic rocks (Heap et al., 2022). These studies, and others, have suggested that whether alteration increases or decreases a certain petrophysical property depends on (1) whether the alteration increases or decreases the porosity of the rock (e.g., through mineral dissolution or porosity-filling mineral precipitation, respectively), a factor known to exert a first-order control on rock physical properties (see review by Heap and Violay, 2021) and (2) whether the secondary (alteration) minerals are characterised by a lower or higher value of the petrophysical property of interest (e.g., in terms of strength, whether the secondary minerals are weaker or stronger than the primary mineral assemblage).

The tensile strength of volcanic rocks is required for analytical or numerical estimates of (1) the magma overpressure required for magma chamber rupture and dyke propagation, (2) the limits on magma chamber volume (see reviews by Gudmundsson, 2006, 2020; Acocella, 2021), and (3) magma under-pressure leading to the generation of collapse-related structures (Folch and Marti, 2004; Holohan et al., 2013). A refined knowledge of the tensile strength of volcanic rocks is also fundamental to improve our understanding of volcanotectonic seismicity during unrest and eruptions (Roman and Cashman, 2018). Volcano stability modelling performed using the finite element method (FEM; Heap et al., 2014; Chen et al., 2017) and the

discrete element method (DEM; Holohan et al., 2015, 2017; Harnett et al., 2018, 2020; Heap and Harnett, 2021), designed to better understand the mechanical behaviour of volcanic rocks and structures, require the tensile strength or the ratio between the compressive and tensile strength as inputs. The tensile strength of volcanic rocks and magmas also exerts crucial control over their fragmentation behaviour (McBirney and Murase, 1970; Alidibirov, 1994; Zhang, 1999; Spieler et al., 2004; Koyaguchi et al., 2008) and is considered a controlling factor in the stability of lava domes (Kilburn, 2018; Harnett et al., 2019). Finally, understanding the tensile strength of volcanic rocks, and in particular altered volcanic rocks, is important for the appraisal and operation of geothermal energy resources in volcanic regions (e.g., Iceland and New Zealand; Arnórsson, 1995; Friðleifsson and Elders, 2005; McNamara et al., 2016; Wilson and Rowland, 2016).

Although experimental studies have shown that the tensile strength of volcanic rocks decreases nonlinearly as a function of porosity (Heap et al., 2012; Lamb et al., 2017; Hornby et al., 2019; Harnett et al., 2019; Kendrick et al., 2021; Heap and Violay, 2021; Heap et al., 2021c; Weydt et al., 2021), and can be influenced by temperature (Hornby et al., 2019; Weaver et al., 2020), the influence of hydrothermal alteration is comparatively understudied. For example, Pola et al. (2014) found that the tensile strength of five lava samples collected from Solfatara (Italy) was reduced from ~12 to ~2 MPa as degree of alteration (determined using the chemical index of alteration, CIA) increased from fresh to completely altered. Mayer et al. (2016) found that the tensile strength of ignimbrites and fall deposits (six blocks in total) from Solfatara and Pisciarelli (Italy) was reduced from ~4.5 to ~0.5 MPa as a function of increasing alteration (determined using the CIA). Despite these initial findings, values of tensile strength for hydrothermally altered rocks are sparse and, to the authors' knowledge, there are no experimental studies that have systemically explored the influence of hydrothermal alteration on the tensile strength of volcanic rocks.

Here, therefore, we present the results of an experimental study in which we performed laboratory tensile experiments on well characterised suites of variably altered volcanic rocks. We first present the experimental material, methods, and results. We then discuss the influence of porosity and alteration on tensile strength, aided by existing theoretical and semi-empirical constitutive models, and discuss the influence of different types of alteration (porosity-increasing dissolution and porosity-decreasing precipitation) on tensile strength. Finally, we highlight the implications of our new data using DEM modelling in which we model fracture localisation following dyke pressurisation within hydrothermally altered host-rock.

2 Materials and Methods

A total of 25 variably altered blocks (typically about 30 × 30 × 30 cm in size) collected from La Soufrière de Guadeloupe (Eastern Caribbean, France), Chaos Crags (California, USA), and Merapi volcano (Indonesia) were used for this study. The collection sites for the blocks are shown on Fig. 1.

A suite of 15 blocks were collected from La Soufrière de Guadeloupe (Fig. 1a), an active andesitic stratovolcano located on the French island of Guadeloupe in the Eastern Caribbean (Komorowski et al., 2005; Moretti et al., 2020). Seven blocks were taken from the collapse scar of the 2009 landslide on the eastern flank of the dome (blocks H2A, H3, H4A, H5A, H6, H29, and H30). Three blocks were collected from the lava spines on the summit of the current lava dome (which formed in 1530 CE): one block from Cratère Sud Central (H19) and two blocks from an adjacent site (H21 and H22). Blocks were also collected from the west wall of the fault "Faille 30 août" (H14 and H15) that cuts the 1530 CE dome, from the scar of an earthquake-triggered landslide (WP1285), and from a lava adjacent to the Galion waterfall (H32). The final block, a volcanic bomb from the 1976–1977 eruption, was taken from the roof of a small disused thermal bathhouse to the south of the dome (WP1317). The blocks from La Soufrière

de Guadeloupe, previously described by Heap et al. (2021a, 2022), are andesites characterised by a porphyritic texture comprising phenocrysts (often a few hundred microns long, but occasionally as large as 1–2 mm) of dominantly plagioclase and pyroxene (orthopyroxene and clinopyroxene) within a crystalline groundmass (Figs. 2a and 2b; Table 1). All samples contain variable quantities of secondary minerals, such as kaolinite, alunite or natro-alunite, silica polymorphs (quartz, cristobalite, tridymite, and opal- A), hematite, pyrite, gypsum, and talc (Table 1).

Five blocks were collected from Chaos Crags (Fig. 1b), a suite of dacitic to rhyodacitic lava domes in the Lassen Volcanic Center (California, USA; Heiken and Eichelberger, 1980; Clynne and Muffler, 2017). All five blocks were collected from Dome C, which collapsed ~350 years ago (Clynne and Muffler, 2017). One block was taken from the tongue-shaped Chaos Jumbles collapse deposit (block CCC), and four blocks were taken from the altered carapace of the dome that now forms the collapse scar (blocks CC3, CC4A, CC4B, and CC10). The blocks from Chaos Crags, previously described by Ryan et al. (2020) and Heap et al. (2021b), are porphyritic rhyodacites containing phenocrysts of dominantly plagioclase, K-feldspar, and quartz within a crystalline groundmass (Figs. 2c and 2d; Table 1). All samples contain variable quantities of secondary minerals (cristobalite, hematite, smectite, and kaolinite; Table 1).

Five blocks were collected from Merapi volcano (Fig. 1c), an active stratovolcano located on the island of Java in Indonesia (Voight et al., 2000; Surono et al., 2012). These blocks (blocks M-U, M-SA1, M-SA2, M-HA1, and M-HA2) were collected from the 1902 dome, ~100 m to the northeast of the currently active dome. The blocks from Merapi volcano, previously described in Heap et al. (2019) and Darmawan et al. (2022), are variably altered basaltic-andesites with a porphyritic texture comprising phenocrysts of dominantly plagioclase and pyroxene within a crystalline groundmass (Figs. 2e and 2f; Table 1). All samples contain

variable quantities of secondary minerals (natro-alunite, alunite, quartz, hematite, cristobalite, gypsum, and various amorphous phases; Table 1).

Because we are interested in exploring the influence of hydrothermal alteration on the tensile strength of volcanic rocks, the alteration assemblage was identified and the alteration intensity of each block was quantified by the weight percentage (wt%) of secondary (i.e. alteration) minerals. The mineral phases present in each block were identified by a combination of optical microscopy, Raman spectroscopy, and X-ray powder diffraction (XRPD). Quantitative phase analysis was then performed using the XRPD data and the Rietveld approach (Bergmann et al., 1998) (Table 1). The data presented in Table 1 were taken from Heap et al. (2019, 2021a, 2022). Backscattered scanning electron microscope (SEM) images of the least- and most-altered blocks from each volcano are provided in Fig. 2. These images, especially those for the samples from La Soufrière de Guadeloupe and Merapi volcano, show that the most-altered samples have much more complex and heterogeneous microstructures (Fig. 2).

Multiple cylindrical samples were cored in the same orientation from each of the rock blocks to a diameter of 20 or 40 mm (based on the volume of material available), and then cut and precision-ground to a nominal length of 20 mm. The rock blocks contained no obvious pore or crystal shape preferred orientation and so the coring direction in each block was selected to maximise the number of cylindrical samples. The samples were washed and then dried in a vacuum-oven at 40 °C for at least 48 h. The connected porosity of each sample was calculated using the bulk sample volume and the skeletal (solid) sample volume measured by a helium pycnometer (an AccuPyc II by Micromeritics©). Measurements of total porosity, determined using the density of a powdered aliquot of each sample (measured using the pycnometer), showed that there is little to no isolated porosity in any of the studied materials. Dry indirect tensile strength was measured on oven-dry samples in a uniaxial loading frame (a LoadTrac II load frame by Geocomp©; Griffiths et al., 2018) using the Brazil disc technique, a method in

200 which samples are deformed diametrically in compression (Fig. 3; Perras and Diederichs,
201 2014). Samples were deformed under ambient laboratory pressure and temperature at a constant
202 displacement rate of 0.025 mm. s^{-1} until the formation of the first macrofracture, which
203 typically occurred during the first 30 s of the experiment. Samples were deformed in a loading
204 platen with curved loading jaws, and a hemispherical ball and seat were used ensure that there
205 was no misalignment (Fig. 3). Axial displacement and axial load were measured using a linear
206 variable differential transducer (LVDT) and a load cell (45 kN maximum), respectively (Fig.
207 3). Indirect tensile strength, σ_t, was then calculated using (Ulusay, 2014):
208
209 $$\sigma_t = \frac{2F}{\pi DL}, \quad (1)$$
210
211 where F is the applied force at the propagation of the first macrofracture, and D and L are the
212 diameter and length of the discs, respectively. The tensile strength data for block CCC from
213 Chaos Crags, and the tensile strength data for four of the five blocks from Merapi volcano
214 (blocks M-U, M-SA1, M-SA2, and M-HA1), were previously published in Heap et al. (2021c).
215
216 **3 Results**
217 Representative force-displacement curves are provided in Fig. 4 for three samples from
218 La Soufrière de Guadeloupe (with high, medium, and low tensile strength), and the tensile
219 strength of the rocks from La Soufrière de Guadeloupe, Chaos Crags, and Merapi volcano are
220 plotted as a function of porosity and alteration in Fig. 5 (all data available in Table 2). In Figs.
221 5a and 5c, the different symbols and colours differentiate the data from the different volcanoes.
222 In Figs. 5b and 5d, the colour of the symbol (where red and yellow indicate low and high values,
223 respectively) indicates the alteration and porosity of the sample, respectively.

The data show that tensile strength is reduced as a function of increasing porosity. For example, tensile strength decreases from ~14 to ~2 MPa as porosity is increased from ~0.05 to almost 0.35 (Fig. 5a). The change in tensile strength as a function of increasing alteration varies between the different sample suites (Fig. 5c). The tensile strength of the andesites from La Soufrière de Guadeloupe decreases as a function of increasing alteration: tensile strength decreases from ~14 to ~4 MPa as alteration is increased from ~6 to ~60 wt% (Fig. 5c). A notable outlier exists in the La Soufrière de Guadeloupe dataset (sample H29_T3; Table 2). This sample has a very low tensile strength of 0.9 MPa, but is not characterised by a high alteration intensity (25.9 wt%). The relative weakness of sample H29_T3 is likely the result of its anomalously high porosity of 0.33 (the porosity of the other samples prepared from this block are 0.27–0.28; Table 2). The tensile strengths of the rhyodacites from Chaos Crags and the basaltic-andesites from Merapi volcano, however, do not appear to vary systematically with increasing alteration (Fig. 5c). For the rocks from Chaos Crags and Merapi volcano, the samples with the lowest tensile strengths are not the most altered samples, and the samples with the highest tensile strengths are not the least altered samples (Fig. 5c).

4 Discussion

4.1 Influence of porosity on the tensile strength of volcanic rocks

New mechanical data show that the tensile strength of variably altered volcanic rocks from La Soufrière de Guadeloupe, Chaos Crags, and Merapi volcano decreases as a function of increasing porosity (Fig. 5a), in accordance with previous studies on volcanic rocks (Heap et al., 2012; Lamb et al., 2017; Hornby et al., 2019; Harnett et al., 2019; Kendrick et al., 2021; Heap and Violay, 2021; Weydt et al., 2021; Heap et al., 2021c).

We compare our new data with those previously published for volcanic rocks (andesites, basalts, dacites, and pyroclastic rocks) in Fig. 6, which shows that our new data are in broad

agreement with those previously published. When all the data are considered, the range of tensile strength for a given porosity can be up to 20–25 MPa (Fig. 6). This range is the result of sample-scale discontinuities (low-porosity samples with a low tensile strength likely contained fractures, for example), microstructural differences (pore diameter, pore aspect ratio, and pore orientation have been shown to influence tensile strength; Heap et al., 2021c), and differences in their degree and type of alteration, as discussed in the next section.

We can further explore the influence of porosity on tensile strength using existing theoretical constitutive models. Constitutive models exist to estimate the critical pressure drop required to rupture bubbly magma (McBirney and Murase, 1970; Alidibirov, 1994; Zhang, 1999; Spieler et al., 2004; Koyaguchi et al., 2008). These micromechanical models describe the tensile bursting of an array of gas-filled solid elastic shells under a given external tensile pressure. However, Heap et al. (2021c) suggested that this critical threshold decompression pressure could be interpreted as akin to the critical bulk tensile strength of porous rock, T, and recast the equations as follows:

$$T \approx \frac{T_0}{\phi} \quad (2a)$$

$$T \approx \frac{T_0(1-1.7\phi)^{\frac{1}{2}}}{\phi} \quad (2b)$$

$$T \approx \frac{2T_0(1-\phi)}{1+2\phi} \quad (2c)$$

$$T \approx \frac{2T_0(1-\phi^n)}{a\phi^n} \quad (2d)$$

$$T \approx \frac{2T_0(1-\phi)}{3\phi\sqrt{\phi^{-1/3}-1}}, \quad (2e)$$

where T_0 is an effective characteristic tensile strength (see Koyaguchi et al., 2008), ϕ is the porosity, and a and n are defined constants (Alidibirov (1994) found a = 1 and n = 1/3, and Koyaguchi et al. (2008) found a = 3 and n = 1). Using a compiled dataset for volcanic rocks, Heap et al. (2021c) assumed that $\sigma_t = T$, and provided best-fit values of T_0 to each of the models given by Eq. (2), found by varying T_0 in such a way as to minimise the sum of square residuals between the logarithm of the data and the logarithm of each model result at the same porosity (Table 3).

In Fig. 7a we show the tensile strength of the rocks from La Soufrière de Guadeloupe, Chaos Crags, and Merapi volcano as a function of porosity, alongside the modelled curves using Eq. (2) and the values of T_0 determined from the previously compiled dataset in Heap et al. (2021c) (Table 3). The modelled curves shown in Fig. 7a underestimate the tensile strength of the rocks measured herein. This underestimation may be due to the numerous low-porosity samples with a low tensile strength in the compiled dataset (Fig. 6). As discussed above, these low-strength samples likely contained sample-scale discontinuities such as fractures, features not present in the samples measured in this study.

We have performed the same fitting procedure described above to provide best-fit values of T_0 for the andesites from La Soufrière de Guadeloupe, the most abundant dataset. Fig. 7b shows the tensile strength of the andesites from La Soufrière de Guadeloupe as a function of porosity, alongside the modelled curves using Eq. (2) and the best-fit values of T_0 for the La Soufrière de Guadeloupe rocks (Table 3). Based on the good description of Eqs. (2d) and (2e) to the La Soufrière de Guadeloupe data (the sums of the square residuals are provided in Table 3), we conclude that these models can be used to estimate the tensile strength of rocks from La

296 Soufrière de Guadeloupe, and perhaps other similarly-altered andesites (using the best-fit values
297 of T_0 provided in Table 3).

298 The similarity between the tensile strength of volcanic rocks and the critical threshold
299 decompression pressure measured from shock-tube experiments (see Heap et al., 2021c)
300 suggests that, in the absence of shock-tube data, the tensile strength data presented herein (Fig.
301 5; Table 2), and/or Eq. (2) and the best-fit values of T_0 (Table 3), can be used to estimate the
302 fragmentation threshold of the studied materials below a porosity of 0.3. Above a porosity of
303 0.3, tensile strength data deviate from fragmentation threshold data from shock-tube
304 experiments due to overpressure leakage (Mueller et al., 2008; Heap et al., 2021c).

305

306 4.2 Influence of alteration on the tensile strength of volcanic rocks

307 New mechanical data show that the tensile strength of the andesites from La Soufrière
308 de Guadeloupe decreases as a function of increasing alteration (Fig. 5c), in accordance with
309 sparse published data for volcanic rocks (Pola et al., 2014; Mayer et al., 2016). However, the
310 tensile strength data for the rocks from Chaos Crags and Merapi volcano do not appear to vary
311 systematically with alteration (Fig. 5c). We highlight that there are fewer samples in the Chaos
312 Crags and Merapi volcano datasets than in the La Soufrière de Guadeloupe dataset, and that the
313 range of alteration intensity measured for the samples from Chaos Crags is smaller than for the
314 other two datasets (Fig. 5c), limitations that could serve to obscure a clear trend in these data.

315 It is unfortunately not possible to replot the compiled data of Fig. 6 as a function of
316 alteration, as the vast majority of studies did not report detailed mineralogical information for
317 their studied materials. Further, because this compilation consists of a combination of unaltered
318 samples, altered samples, and samples for which there is no information, it is challenging to
319 assess the role of alteration using the compiled dataset, or by comparing our new data with the
320 compiled data. Aided by ancillary data, microstructural observations, and comparisons with

published data, we will now discuss the influence of alteration on the three suites of rocks measured herein.

Our new data for the rocks from La Soufrière de Guadeloupe are in agreement with the conclusions of previous studies, which suggest that alteration decreases the tensile strength of volcanic rocks (Pola et al., 2014; Mayer et al., 2016). We also note that the uniaxial compressive strength, a strength parameter that is typically 10 or 12 times higher than the tensile strength (Cai, 2010), of these same rocks from La Soufrière de Guadeloupe was also found to decrease as a function of increasing alteration (Heap et al., 2021a).

One possible reason for the measured reduction in the tensile strength of the samples from La Soufrière de Guadeloupe as a function of alteration is that the secondary mineral assemblage is likely weaker than the primary mineral assemblage. Indeed, it was argued by Heap et al. (2021a) that the reduction in compressive strength of these rocks as a function of alteration was the result of the relative weakness of the secondary mineral assemblage and, in particular, the presence of clay minerals. Clay minerals, abundant in these rocks (Table 1), have been previously considered by several authors to reduce the overall strength of volcanic rocks (del Potro and Hürlimann, 2009; Nicolas et al., 2020; Opfergelt et al., 2006; Watters and Delahaut, 1995).

Another possible reason for the measured reduction in the tensile strength is that hydrothermal alteration has increased the microstructural heterogeneity of the rocks (as shown in the SEM images of Figs. 2 and 8). Microstructural heterogeneity has been previously shown to reduce the strength of rocks (Tang et al., 2007; Villeneuve et al., 2012; Heap et al., 2016; Peng et al., 2017; Xu et al., 2020).

A final possible reason for the reduction in the tensile strength of the samples from La Soufrière de Guadeloupe as a function of alteration is that the alteration could have increased porosity the samples, a factor known to greatly influence tensile strength (Fig. 6; Heap et al.,

2012; Lamb et al., 2017; Hornby et al., 2019; Harnett et al., 2019; Kendrick et al., 2021; Heap and Violay, 2021; Weydt et al., 2021; Heap et al., 2021c). Indeed, the porosity of the andesites from La Soufrière de Guadeloupe increases as a function of alteration (Fig. 9; see also Figs. 5c and 5d). However, a microstructural inspection of the andesites from La Soufrière de Guadeloupe shows that the alteration is characterised by both porosity-increasing alteration (mineral dissolution leading to the formation of pores), especially in plagioclase crystals (Figs. 8a and 8b), and porosity-decreasing alteration (pore- and crack-filling mineral precipitation by Na-alunite and silica polymorphs; Fig. 8c). Therefore, it is unclear from these data and observations whether the alteration has increased the porosity of the samples from La Soufrière de Guadeloupe (as suggested by Fig. 9), or whether the more porous samples are simply more altered due to their higher fluid-rock ratios. As a result, it is challenging to separate the influence of porosity and alteration on tensile strength and draw firm conclusions as to the influence of alteration. Studies that alter volcanic rocks under controlled laboratory conditions and then measure their tensile strengths would be required to separate the contributions of porosity and alteration on the tensile strength of volcanic rocks. For example, Farquharson et al. (2019), altered samples in the laboratory by immersing them in a bath of sulphuric acid and found that alteration increased the porosity and decreased the uniaxial compressive strength of andesite.

Although we cannot draw firm conclusions as to influence of alteration on the tensile strength of the andesites from La Soufrière de Guadeloupe, because of the aforementioned link between porosity and alteration, we speculate that hydrothermal alteration has reduced their tensile strength due to the relative weakness of the secondary mineral assemblage (Table 1) and the increase in microstructural heterogeneity that accompanies hydrothermal alteration (Figs. 2 and 8).

The tensile strength of the basaltic-andesites from Merapi volcano does not appear to vary systematically with alteration (Fig. 5c). The block with the highest tensile strength (~10

MPa; block M-SA2) is not the least altered block, and the block with the lowest tensile strength (~2–3 MPa; block M-SA1) is not the most altered block (Fig. 5c; Table 2). The high tensile strength of block M-SA2 is likely due a combination of its low porosity (Table 2) and an alteration assemblage that is not dominated by low-strength secondary minerals (Table 1), and the low tensile strength of block M-SA1 can be explained by its high porosity (Table 2). Similar to the andesites from La Soufrière de Guadeloupe, although the porosity of the basaltic-andesites from Merapi volcano appears to increase as a function of increasing alteration (Fig. 9), they are characterised by both porosity-increasing (Fig. 8h) and porosity-decreasing (Figs. 8f and 8g) alteration. It is also unclear, as for the andesites from La Soufrière de Guadeloupe, whether the alteration has increased the porosity of the samples from Merapi volcano, or whether the more porous samples are simply more altered. Because of the similarities in alteration assemblage and microstructure between the rocks from La Soufrière de Guadeloupe and Merapi volcano, we anticipate, if more data were available, that the rocks from Merapi volcano would also show a similar trend of decreasing tensile strength as a function of alteration. Indeed, Darmawan et al. (2022) concluded that the uniaxial compressive strength of altered rocks from Merapi volcano, including some of the samples tested here, decreased as a function of increasing alteration due to the relative weakness of the secondary mineral assemblage.

The tensile strength of the rhyodacites from Chaos Crags also does not appear to vary systematically with alteration (Fig. 5c). The block with the highest tensile strength (~7–8 MPa; block CC4A) is not the least altered block, and the block with the lowest tensile strength (~3–4 MPa; block CC4B) is not the most altered (Fig. 5c; Table 2; although some samples from blocks CC3 and CC10 also have a tensile strength of ~3–4 MPa). In a previous study, Heap et al. (2021b) found that the uniaxial compressive strength of block CC4A was considerably higher than for the other rocks from Chaos Crags (~120−140 MPa, compared to ~40−55 MPa).

These authors suggested that pore- and crack-filling alteration in sample CC4A (Fig. 8d and 8e) was responsible for the observed increase in uniaxial compressive strength (Heap et al., 2021b). Unlike the rocks from La Soufrière de Guadeloupe and Merapi volcano, block CC4A from Chaos Crags does not contain abundant porosity-increasing alteration (i.e. mineral dissolution). Therefore, we conclude here that the high tensile strength of block CC4A is likely to be the result of pore- and crack-filling alteration (Fig. 8d and 8e), which has reduced the porosity of this block (Table 2). As discussed above, this same conclusion was drawn to explain the higher compressive strength of block CC4A in Heap et al. (2021b).

Although it is difficult to draw firm conclusions as to the influence of alteration on the tensile strength of volcanic rocks, because porosity and alteration influence each other, we conclude that it is likely that hydrothermal alteration has modified the tensile strength of the rocks collected from La Soufrière de Guadeloupe, Chaos Crags, and Merapi volcano, and in different ways. The alteration of the rocks from La Soufrière de Guadeloupe and Merapi volcano, which we consider to have reduced tensile strength, manifests as both porosity-increasing (dissolution) and porosity-decreasing (pore- and crack-filling mineral precipitation) alteration (Fig. 8), and is characterised by a relatively weak secondary mineral assemblage consisting of minerals such as clays (Table 1) and an increase in microstructural heterogeneity (Figs. 2 and 8). The alteration of one of the blocks from Chaos Crags, which we consider to have increased tensile strength, is characterised by pore- and crack-filling mineral precipitation and an absence of the dissolution textures that typify the samples from La Soufrière de Guadeloupe and Merapi volcano (Fig. 8). We conclude, therefore, that not only does alteration likely influence the tensile strength of volcanic rocks, but also that the type of alteration (porosity-increasing or porosity-decreasing alteration, and the alteration minerals involved) likely dictates whether the alteration decreases or increases the tensile strength.

The constitutive models presented in Eq. (2) provide estimates for the tensile strength when the porosity and an effective characteristic tensile strength, T_0, is known. However, some volcano monitoring methods, such as remote sensing (Kereszturi et al., 2020; Mueller et al., 2021), provide the extent and intensity of hydrothermal alteration. To assist volcano monitoring efforts, we can adapt Eq. (2) so that tensile strength can be estimated for a given degree of alteration, rather than for a given porosity. To do so, we focus on the data for the andesites from La Soufrière de Guadeloupe, the most abundant dataset. The relationship between porosity and alteration (Fig. 9) can be described by a simple power law of the form $\phi = c_1 A^{c_2}$, where A is the alteration (in wt%). We fit for the two constants c_1 and c_2 using a least squares minimization of the power law $\gamma = f(A)$ to the La Soufrière de Guadeloupe subset of the data in Fig. 9. By this method, we find that c_1 =0.0252 wt.% and c_2 =0.5660, respectively, for the data for La Soufrière de Guadeloupe. The term $c_1 A^{c_2}$ can then be substituted for ϕ in Eq. (2) to yield a sequence of expressions for T that depend on A and the constants T_0, c_1, and c_2, all of which are found independently,

$$T \approx \frac{T_0 A^{-c_2}}{c_1} \quad (3a)$$

$$T \approx \frac{T_0 A^{-c_2}(1 - 1.7A^{c_2})^{\frac{1}{2}}}{c_1} \quad (3b)$$

$$T \approx T_0 \left(\frac{3}{2c_1 A^{c_2} + 1} - 1\right) \quad (3c)$$

$$T \approx \frac{2T_0((c_1 A^{c_2})^{-n} - 1)}{a} \quad (3d)$$

443 $$T \approx \frac{2T_0 A^{-c_2}(1 - c_1 A^{c_2})}{3c_1\sqrt{(c_1 A^{c_2})^{-1/3} - 1}}. \quad (3e)$$

444

445 We show in Fig. 10 the experimental data for La Soufrière de Guadeloupe alongside the
446 modelled curves for Eq. (3). As for Fig. 7b, we use the best-fit values of T_0 for the La Soufrière
447 de Guadeloupe data, provided in Table 3. Based on the good description of these models to the
448 La Soufrière de Guadeloupe data, we conclude that it is also possible to provide tensile strength
449 estimates for andesites from La Soufrière de Guadeloupe using the degree of alteration, rather
450 than the porosity (using the best-fit values of T_0 provided in Table 3 and c_1 and c_2 found via
451 Fig. 9). It is recommended here that Eqs. (3d) and (3e) are used preferentially, due to their low
452 sum of square residuals to the data (provided in Table 3). As discussed above, Eq. (3) and the
453 best-fit values of T_0 (Table 3) could also be used to estimate the fragmentation threshold of the
454 studied materials below a porosity of 0.3. We again highlight that the outlier on Fig. 10 (sample
455 H29_T3), which has a very low tensile strength compared to its alteration intensity, is likely the
456 result of its anomalously high porosity (see Table 2 and the discussion above).

457

458 4.3 Implications

459 Our experimental study provides values of tensile strength for hydrothermally altered
460 volcanic rocks (Fig. 5). As noted above, the tensile strength of volcanic rocks is required for
461 estimates of (1) the magma overpressure required for magma chamber rupture and dyke
462 propagation, (2) the limits on magma chamber volume, (3) magma under-pressure leading to
463 the generation of collapse-related structures, and (4) process-based models of the nature and
464 dynamics of volcanotectonic seismicity during unrest and eruptive phases. Because the rocks
465 adjacent to a magma chamber or dyke are likely to be hydrothermally altered (e.g., Goto et al.,
466 2008; Salaün et al., 2011; Mordensky et al., 2018; Yilmaz et al., 2021), we propose that the
467 tensile strengths of altered volcanic rocks, documented here, are perhaps the most suited to

provide estimates of dyke and magma chamber overpressure and magma chamber volume. Similarly, the volcanic rocks in geothermal reservoirs are also often hydrothermally altered (e.g., Browne, 1978; Marks et al., 2010; Siratovich et al., 2014; Cant et al., 2018; Lévy et al., 2018; Heap et al., 2020) and so we propose that modelling designed to, for example, guide reservoir stimulation strategies should also consider tensile strength values for hydrothermally altered volcanic rocks.

FEM (Heap et al., 2014; Chen et al., 2017) and DEM (Holohan et al., 2017; Harnett et al., 2018, 2020; Heap and Harnett, 2021) models designed to better understand the mechanical behaviour of volcanic rocks and structures also require a robust value for the tensile strength of volcanic rock. However, it is more common to use a laboratory-measured uniaxial compressive strength and then assume a ratio, typically 10 or 12, between the compressive and tensile strength. To assist such modelling, we provide here the range of compressive to tensile strength ratios for our studied materials (Table 4; Fig. 11a) and investigate whether this ratio varies systematically as a function of porosity (Fig. 11b) or alteration (Fig. 11c).

We find that the ratio of compressive to tensile strength for the volcanic rocks studied here is between ~5 and ~20, and that uniaxial compressive strength increases as a function of tensile strength (Fig. 11a; Table 4). This ratio range is similar to that provided by Cai (2010), who showed that it varied from 4 to 40 for a range of rock types (with a mode ratio of 14). Fig. 11 shows that the ratio of compressive to tensile strength does not vary systematically as a function of porosity or alteration. Nevertheless, our data (Table 4) show that (1) the accuracy of FEM and DEM models could be improved by using laboratory-measured values for both uniaxial compressive and tensile strength and (2) if tensile strength is unknown, there is justification for running models using a wide range of compressive to tensile strength ratios.

The above discussion prompts the following questions. (1) How do changes in the tensile strength of hydrothermally altered volcanic rocks influence large-scale volcanic

processes? (2) How are the predictions from large-scale modelling influenced by changing the ratio of compressive to tensile strength? To tackle these questions, we developed two-dimensional DEM models in Particle Flow Code (PFC; Itasca Consulting Group, Inc.) capable of reproducing solid and brittle rock behaviour and deformation. The aim of the models is to investigate host-rock damage accumulation and distribution in response to the pressurisation of a dyke-like magma body. A packed particle assemblage was created following the procedure outlined by Potyondy and Cundall (2004), after which contact bonds were installed between the particles forming the host-rock (coloured grey in the resultant figures) to create a bonded particle assemblage capable of reproducing solid rock behaviour (Potyondy and Cundall, 2004; Potyondy, 2012). The dyke, a 700 m-long and 100 m-wide penny-shaped crack, was located at a depth of 300 m within a homogeneous host-rock. The particles within the dyke (coloured red in the resultant figures) remained unbonded, to simulate fluid-like properties. The assemblage was then settled under a gravitational acceleration of 9.81 m/s^2, following the procedure outlined in Holohan et al. (2011). Dyke pressurisation was implemented within the model by increasing the radii of the particles within the dyke by a set factor, leading to a constant incremental area increase (an area increase of 1% was used for the models presented here). Damage accumulation in the host-rock is visualised in the models by examining interparticle bond breakage. Bond breakage (shown by black lines in the resultant figures) occurs when local stresses exceed the cohesive or tensile strength of the individual contacts between particles. We can then quantify this damage as a proportion of the still-bonded contacts in the model. We highlight that our modelling does not consider temperature-induced changes to the physical and mechanical properties of the host-rock adjacent to the dyke. High-temperatures can promote thermal microcracking and/or chemical or phase transformations that can reduce, for example, strength and Young's modulus (Heap and Violay, 2021).

To address the first question above, and as guided by our laboratory data and observations, the mechanical properties of the homogeneous host-rock were chosen to simulate three key scenarios: (1) weak hydrothermally altered host-rock, (2) unaltered or intact rock, and (3) strong hydrothermally altered host-rock. To ensure that the bulk behaviour of the particle-based model accurately represents the laboratory data, we performed an iterative calibration procedure (further outlined in Holohan et al., 2011; Potyondy, 2016; Harnett and Heap, 2021), details of which can be found in the Supplementary Material. The input parameters (the target input parameters and those resulting from the calibration procedure) for the modelling are provided in Table 5.

We show the model results for each of the three scenarios ("intact", "altered weak", and "altered strong") in Fig. 12. We can quantify the damage accumulated due to dyke pressurisation in each case by calculating the number of broken contacts as a proportion of initial bonded contacts in the gravitationally stable model. We find the following proportions of damage in each scenario: (1) 2.9% microcracking in the intact host-rock (Fig. 12b), (2) 6.5% microcracking in the weak hydrothermally altered host-rock (Fig. 12a), and (3) 1.6% microcracking in strong hydrothermally altered host-rock (Fig. 12c). In other words, weak hydrothermally altered host-rock will be more pervasively damaged than unaltered host-rock, and strong hydrothermally altered host-rock will be less damaged than unaltered host-rock. We highlight that our modelling assumes that the host-rock is brittle and that weak hydrothermally altered host-rock could reduce the number of microcracks relative to the unaltered case if the rock is able to deform in a ductile manner (Mordensky et al., 2019). Our modelling also shows that (1) the damage is more widespread in the weak hydrothermally altered host-rock (Fig. 12a), and, conversely, damage is more localised in the strong hydrothermally altered host-rock (Fig. 12c) and (2) the number of fractures that reach the surface increases when the host-rock is weak, and decreases when the host-rock is strong (Fig. 12).

To address the second question, the ratio of compressive to tensile strength of the homogeneous host-rock was varied between 5 and 20 (guided by our experimental data; Table 4), whilst maintaining a constant Young's modulus of 30 GPa and a constant uniaxial compressive strength of 100 MPa (i.e. we only varied the tensile strength). A compressive to tensile strength ratio of 10 represents the same host-rock properties as the "intact" state shown in Fig. 12. We again performed an iterative calibration procedure, details of which can be found in the Supplementary Material. The input parameters (the target input parameters and those resulting from the calibration procedure) for the modelling are provided in Table 6. The model results are presented in Fig. 13. We find the following proportions of damage in each scenario: (1) 0.9% microcracking in the host-rock with a ratio of 5 (Fig. 13a), (2) 2.9% microcracking in the host-rock with a ratio of 10 (Fig. 13b), and (3) 7.8% microcracking in the host-rock with a ratio of 20 (Fig. 13c). In other words, increasing the ratio of compressive to tensile strength (i.e. decreasing the tensile strength) results in a more pervasively damaged host-rock. Our modelling also shows that (1) damage is more widespread as the ratio of compressive to tensile strength increases and (2) the number of fractures that reach the surface remains the same for ratios tested here (Fig. 13).

Taken together, our DEM modelling shows that the extent and spatial distribution of damage surrounding a pressurised source is different for weak and strong hydrothermally altered host-rock (Figs. 12 and 13), with implications for the nature and dynamics of volcanotectonic seismicity during unrest and eruptive phases (Roman and Cashman, 2008). For example, the hundreds of shallow (i.e. within the hydrothermal system), low-magnitude earthquakes at La Soufrière de Guadeloupe each month (Moretti et al., 2020) could be, in part, due to the alteration of the rock hosting the hydrothermal system. We also note that a weak hydrothermally altered host-rock may also provide a greater number of paths to the surface, which could be used for, for example, the escape of hydrothermal fluids (e.g., as fumaroles).

Improving the circulation of hydrothermal fluids may increase the efficiency and extent of the alteration, further influencing the physical and mechanical properties of the host-rocks. A greater number of larger fractures may also help create viable geothermal and epithermal mineral resources by increasing permeability and channelising the flow of hydrothermal fluids, respectively (Rowland and Simmons, 2012; Heap et al., 2020). Taken together, these models suggest that alteration induced changes to tensile strength should be considered in the large-scale modelling of volcanic and geothermal systems.

5 Conclusions and future work

Motivated by the common occurrence of hydrothermal alteration at volcanic and geothermal systems, the need for reliable values of tensile strength for modelling, and the paucity of laboratory data, we performed a systematic study designed to (1) provide values for the tensile strength of hydrothermally altered volcanic rocks and (2) to explore the influence of alteration on the tensile strength of volcanic rocks. Our study shows that the tensile strength of volcanic rocks decreases as a function of porosity (Figs. 5a and 5b), in accordance with previous studies (Fig. 6), and as a function of alteration (Figs. 5c and 5d). However, it is challenging to separate the influence of porosity and alteration on tensile strength, because the initial porosity influences the alteration intensity due to the higher fluid-rock ratio, and the alteration influences the porosity (Fig. 8). While the influence of porosity on the tensile strength of volcanic rocks is well-established (Fig. 6), we use our new data and observations to speculate on the influence of alteration on the tensile strength of volcanic rocks. Taken together, our data and observations suggest that hydrothermal alteration could increase or decrease tensile strength, depending on the type of alteration. Decreases in tensile strength following alteration are thought to be the result of mineral dissolution, the replacement of primary minerals with weak secondary minerals (such as clays), and an increase in microstructure heterogeneity. Increases in tensile

strength following alteration are thought to be the result of pore- and crack-filling mineral precipitation.

Large-scale simulations using DEM models, guided by our experimental results, shows that the tensile strength of hydrothermally altered volcanic rocks influences the extent and spatial distribution of damage surrounding a pressurised source (Figs. 12 and 13). Our modelling therefore emphasises that the tensile strengths of altered volcanic rocks should be used in models designed to better understand volcanic processes and in the development of strategies designed to increase the efficiency of volcanic geothermal reservoirs, systems often characterised by pervasive hydrothermal alteration.

To conclude, our study suggests that mapping the extent and evolution of hydrothermal systems is important to inform modelling endeavours (using, for example, electrical methods; Rosas-Carbajal et al., 2016; Byrdina et al., 2017; Ghorbani et al., 2018; Soueid Ahmed et al., 2018), and that future research should focus on understanding and modelling the geophysical and geochemical signatures of alteration associated with rock weakening and rock strengthening. Future experimental studies should focus on (1) measuring the tensile strength of volcanic rocks that have been altered in the laboratory to preserve different alteration intensities and (2) determining the influence of water-saturation and temperature on the tensile strength of hydrothermally altered volcanic rocks, factors known to influence the mechanical behaviour of volcanic rocks (Heap and Violay, 2021).

Acknowledgements

This work was supported by the TelluS Program of INSU-CNRS ("Assessing the role of hydrothermal alteration on volcanic hazards") and ANR grant MYGALE ("Modelling the phYsical and chemical Gradients of hydrothermal ALteration for warning systems of flank collapse at Explosive volcanoes"), awarded to the first author. MJH also acknowledges support

from the Institut Universitaire de France (IUF). CH and MJH acknowledge support from the Irish Research Council (IRC), the French ministries for Europe and foreign affairs (MEAE and higher education, research and innovation (MESRI), and Campus France via the Hubert Curien (PHC) Ulysses Ireland-France funding scheme. We thank the IPGP for general funding for the Observatoires Volcanologiques et Sismologiques (OVS), INSU-CNRS for the funding provided by the Service National d'Observation en Volcanologie (SNOV), and the Ministère pour la Transition Ecologique (MTE) for financial support for the monitoring of the instable flank of La Soufrière de Guadeloupe. This study contributes to the IdEx Université de Paris ANR-18-IDEX-0001. Material collection from Chaos Crags as permitted by the United States National Park Service (study: LAVO-00050; permit: LAVO-2019-SCI-0010), and we thank Kelly Russell, Stephan Kolzenburg, Lori Kennedy, Martin Harris, and Michael Clynne for their help and support. Samples from Merapi were collected within the framework of the Indonesia-German SUNDAARC agreement and this work represents a contribution to the GEOTECHNOLOGIEN program by BMBF and DFG (Grant 03G0578A). Aurélien Honegger and Marie Violay at EPFL (Switzerland) are thanked for performing the uniaxial compressive strength tests on sample H32. The constructive comments of Jessica Ball and one anonymous reviewer helped improve this manuscript.

CRediT author statement

Michael J. Heap: Conceptualization; Methodology; Formal analysis; Investigation; Resources; Writing - Original draft; Visualization; Supervision; Project administration; Funding acquisition

Claire Harnett: Conceptualization; Methodology; Software; Formal analysis; Writing - Original draft; Investigation; Visualization

Fabian Wadsworth: Conceptualization; Methodology; Formal analysis; Writing - Review & Editing

H. Albert Gilg: Investigation; Writing - Review & Editing

Lucille Carbillet: Investigation; Resources; Writing - Review & Editing

Marina Rosas-Carbajal: Resources; Writing - Review & Editing; Project administration; Funding acquisition

Jean-Christophe Komorowski: Resources; Writing - Review & Editing; Project administration; Funding acquisition

Patrick Baud: Resources; Writing - Review & Editing

Valentin Troll: Resources; Writing - Review & Editing

Frances Deegan: Resources; Writing - Review & Editing

Eoghan Holohan: Methodology; Software; Writing - Review & Editing

Roberto Moretti: Resources; Project administration; Writing - Review & Editing

Fig. 1. Sample collection sites. Images of (a) La Soufrière de Guadeloupe (Eastern Caribbean, France), (b) Chaos Crags (California, USA), and (c) Merapi volcano (Java, Indonesia) showing the location of the sample collection sites (from Earth data ©2019 Google). Insets show maps of Guadeloupe, California, and Java, respectively, with the volcanoes indicated by red triangles. Global Positioning System (GPS) coordinates for the sampling sites are provided in the Supplementary Material.

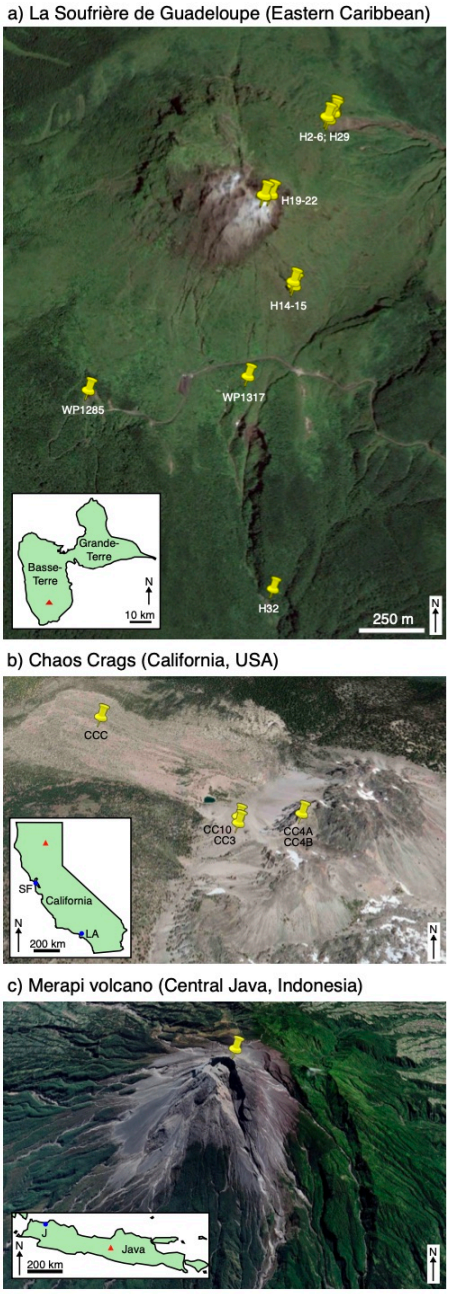

Fig. 2. Backscattered scanning electron microscope (SEM) of the least- and most-altered rocks from each volcano (based on the weight percentage of secondary minerals, indicated above each image). La Soufrière de Guadeloupe – H32 (least altered) and H19 (most altered); Chaos Crags – CCC (least altered) and CC4A (most altered); Merapi volcano – M-U (least altered) and M-HA2 (most altered).

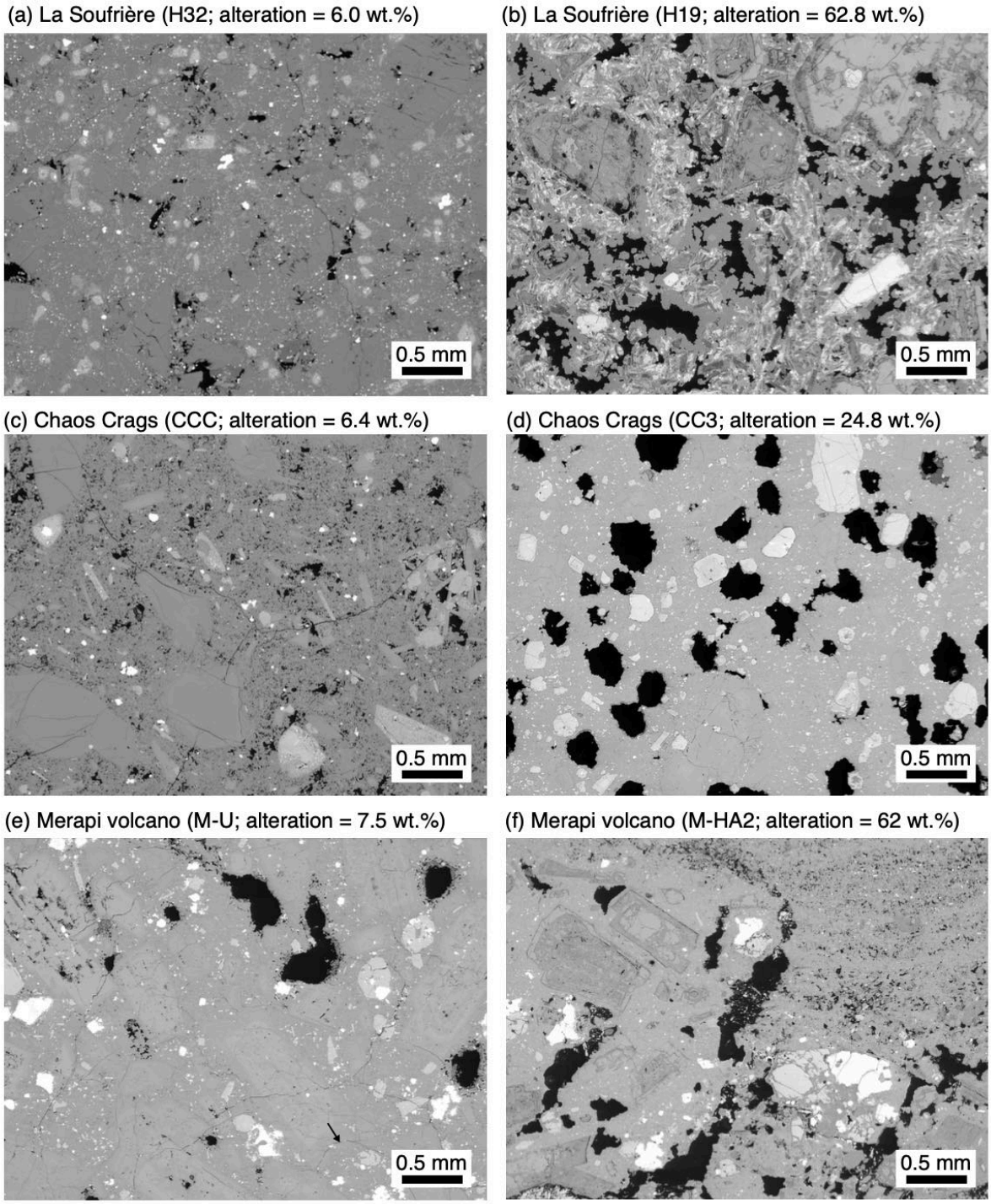

669 **Fig. 3.** Schematic diagram of the experimental setup to measure the tensile strength of rocks
670 (not to scale). LVDT – linear variable differential transducer. The setup is approximately 2 m
671 in height.

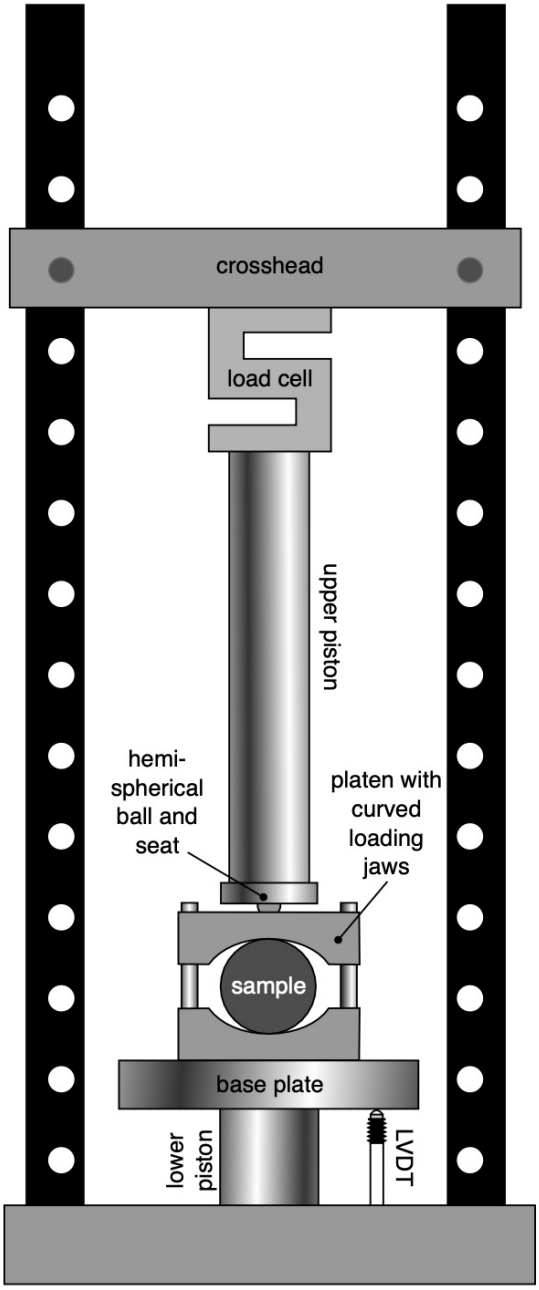

672

673

674 **Fig. 4.** Representative force-displacement curves for three of the samples (all from La Soufrière
675 de Guadeloupe; Table 2) deformed for this study.

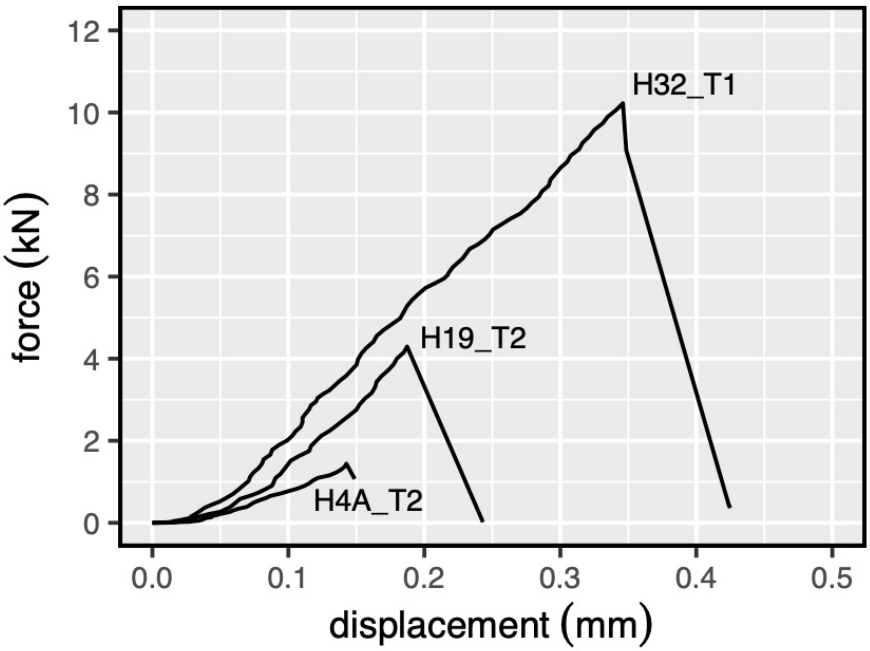

676

677

Fig. 5. Panels (a) and (b) show the tensile strength as a function of porosity. Panels (c) and (d) show the tensile strength as a function of alteration (the weight percentage of secondary minerals). For panels (a) and (c), La Soufrière de Guadeloupe – black circles; Chaos Crags – red squares; Merapi volcano – green triangles. For panels (b) and (d), the colour of the symbol indicates the alteration and porosity, respectively. Experimental errors for the measurements of porosity and tensile strength are < 1% (i.e. within the symbol size). Relative errors for the weight percentages are 5–10%.

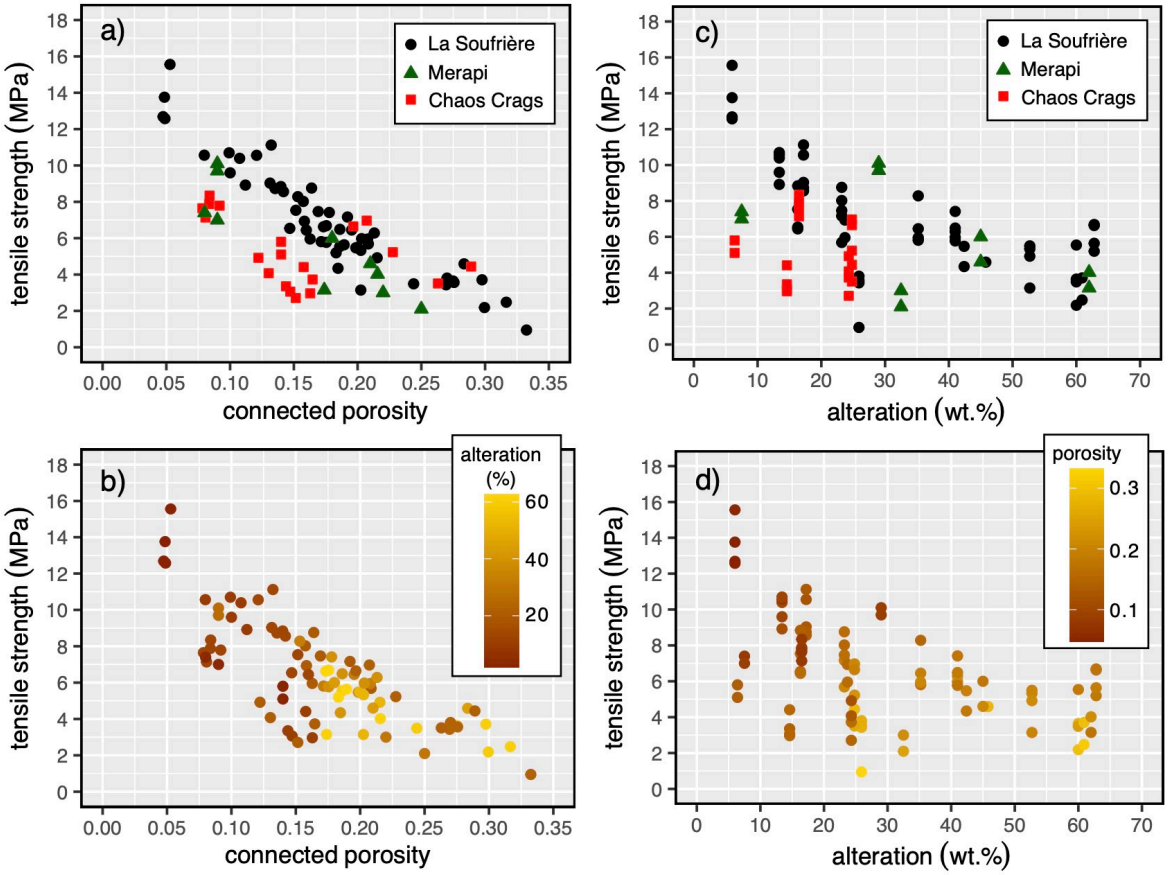

Fig. 6. Tensile strength as a function of porosity for andesites from La Soufrière de Guadeloupe (black circles), rhyodacites from Chaos Crags (red squares), basaltic-andesites from Merapi volcano (green triangles), and compiled data from the literature (andesites, basalts, dacites, and pyroclastic rocks; grey circles). Literature data from: Tuğrul and Gürpinar (1997), Gupta and Rao (2000), Chen et al. (2004), Ersoy and Atici (2007), Kılıç and Teymen (2008), Nara et al. (2010), Kahraman and Yeken (2010), Graue et al. (2011), Lavallée et al. (2012), Heap et al. (2012), Wedekind et al. (2013), Karakuş and Akatay (2013), Hashiba and Fukui (2015), Siratovich et al. (2015), Fener and Ince (2015), Ündül and Er (2017), Yavuz et al. (2017), Lamb et al. (2017), Malik et al. (2017), Aldeeky and Al Hattamleh (2018), Zorn et al. (2018), Hornby et al. (2019), Harnett et al. (2019), Moon and Yang (2020), Yasar and Komurlu (2020), Kendrick et al. (2021), Heap et al. (2021c), and Weydt et al. (2021).

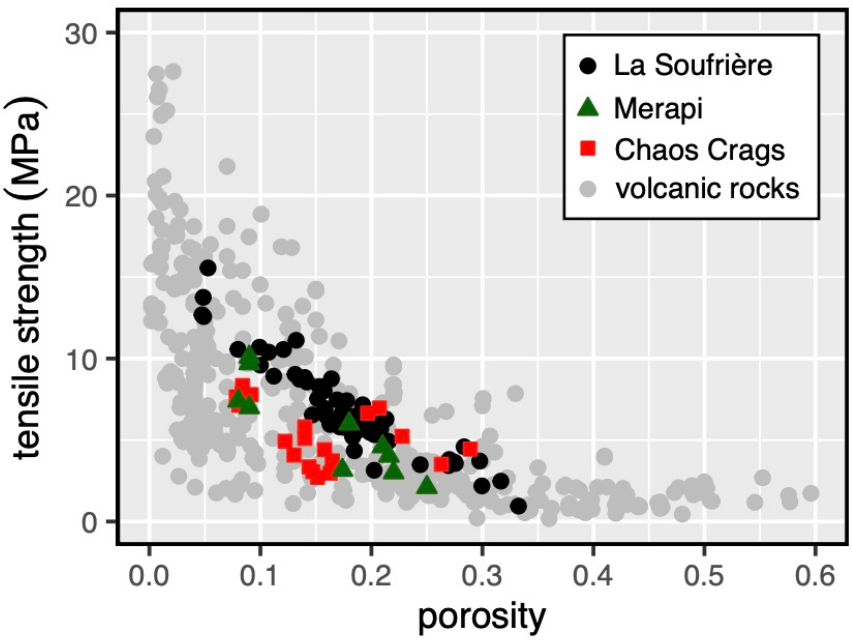

Fig. 7. (a) Tensile strength as a function of porosity for andesites from La Soufrière de Guadeloupe (black circles), rhyodacites from Chaos Crags (red squares), and basaltic-andesites from Merapi volcano (green triangles). Modelled curves are provided using Eq. (2), using the best-fit T_0 for a previously compiled dataset (Table 3). (b) Tensile strength as a function of porosity for andesites from La Soufrière de Guadeloupe (black circles). Modelled curves are provided using Equation (2), using an updated best-fit T_0 for the rocks from La Soufrière de Guadeloupe (Table 3).

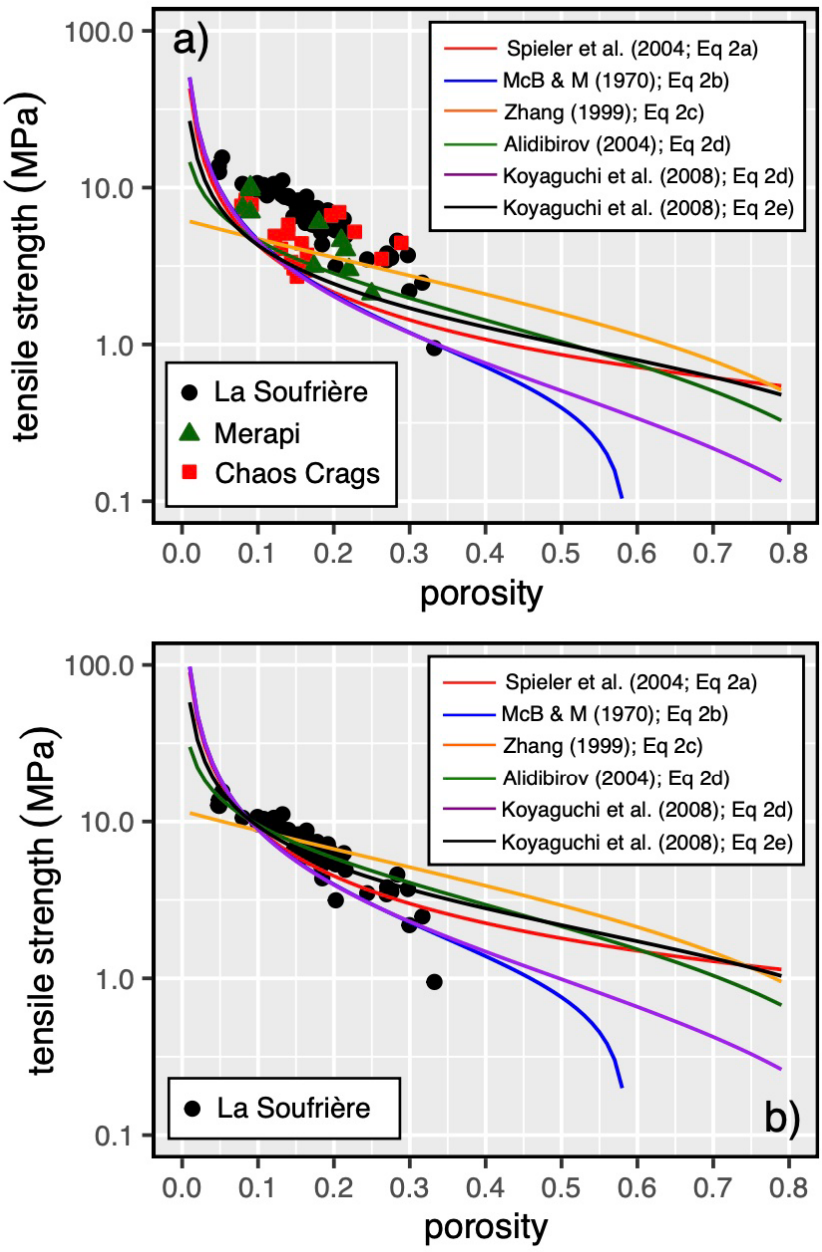

Fig. 8. Backscattered scanning electron microscope (SEM) images of samples from La Soufrière de Guadeloupe (a-c), Chaos Crags (d-e), and Merapi volcano (f-h) showing examples of porosity-increasing (e.g., the dissolution of plagioclase crystals causing "sieve" textures) and porosity-decreasing (crack- and pore-filling precipitation) alteration.

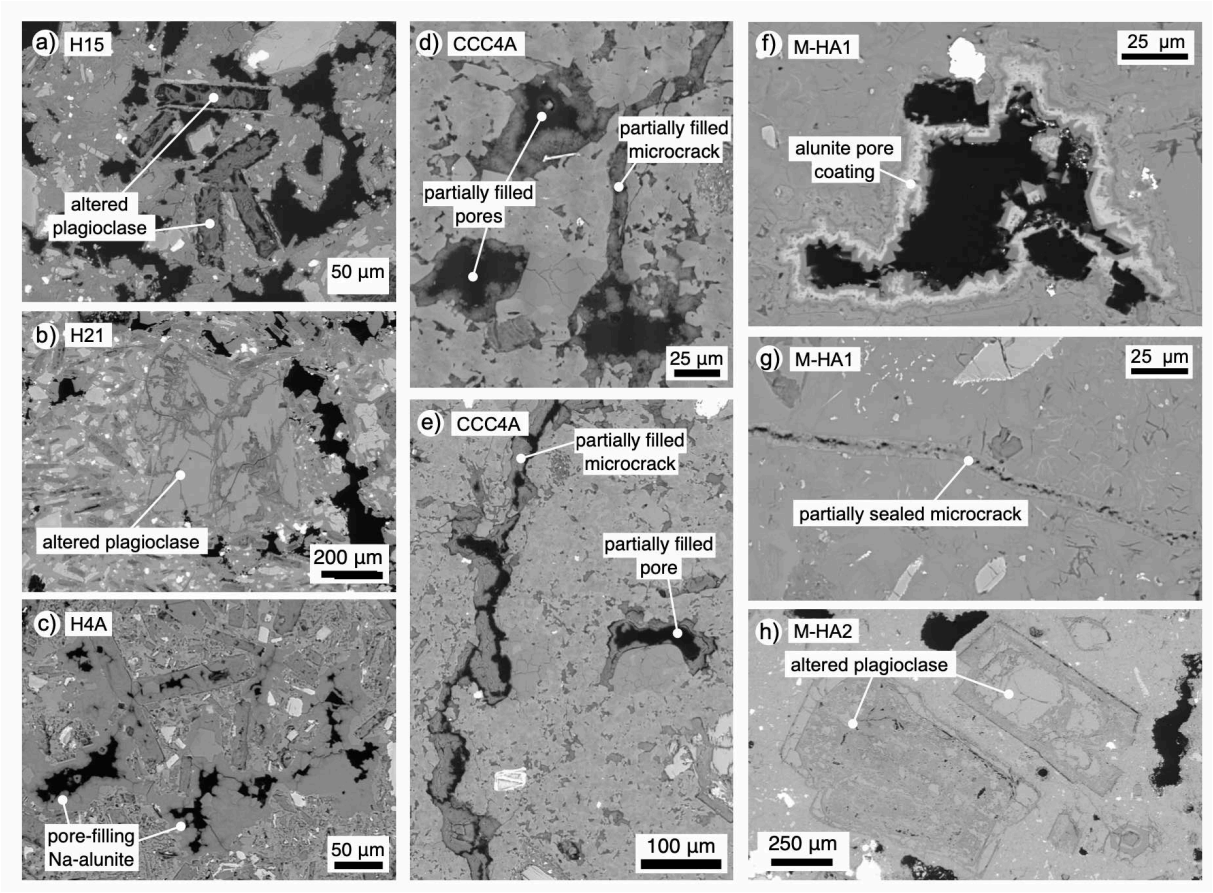

Fig. 9. Connected porosity as a function of alteration (the weight percentage of secondary minerals). La Soufrière de Guadeloupe – black circles; Chaos Crags – red squares; Merapi volcano – green triangles.

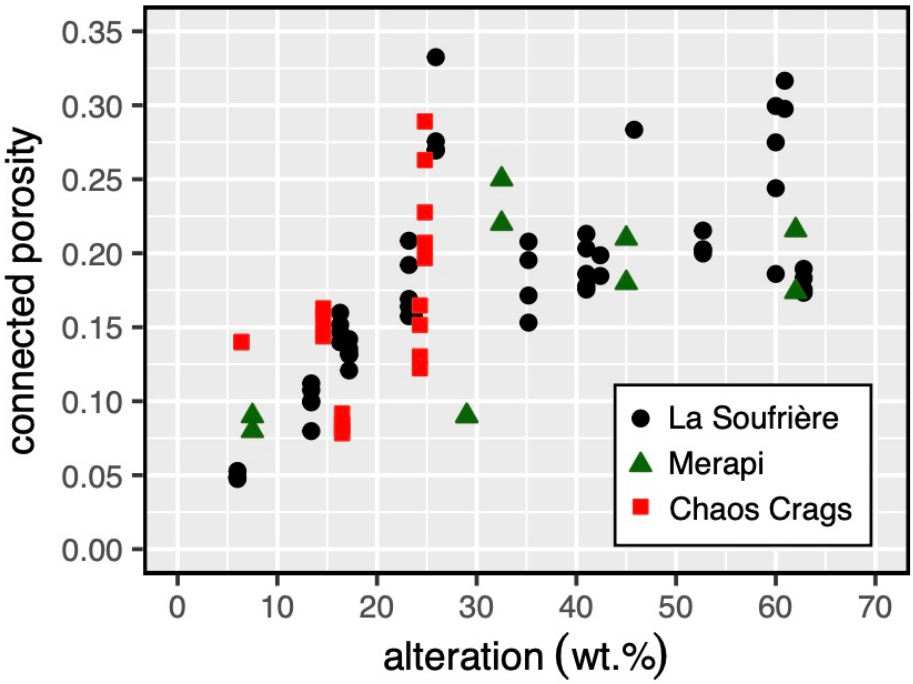

719 **Fig. 10.** Tensile strength as a function of alteration (weight percentage of secondary minerals)
720 for andesites from La Soufrière de Guadeloupe (black circles). Modelled curves are provided
721 using Equation (3), which is a modified version of the equations provided in the referenced
722 studies, using the best-fit T_0 for the rocks from La Soufrière de Guadeloupe (Table 3).

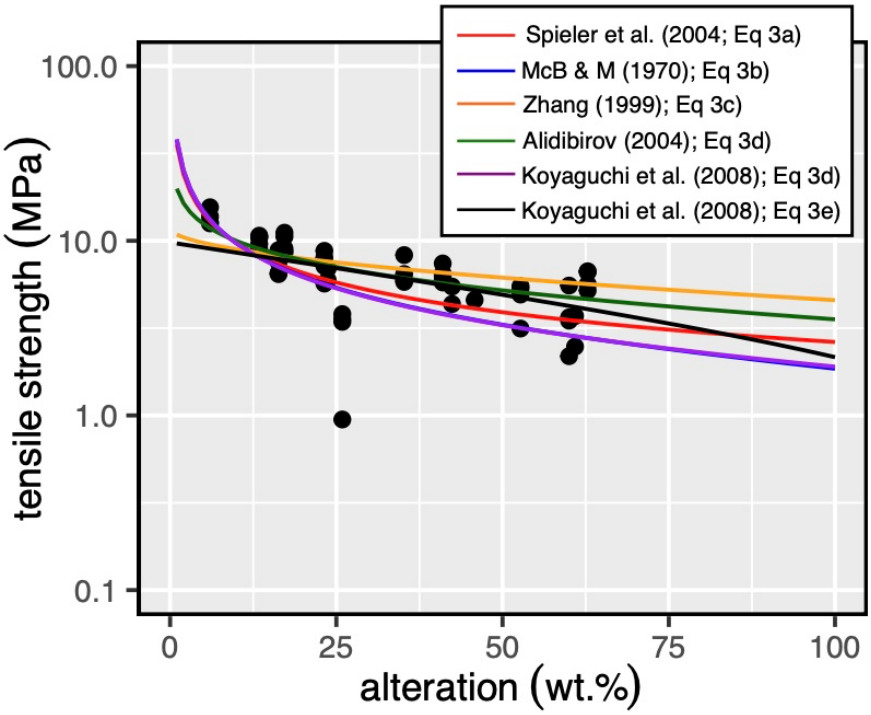

723

724

Fig. 11. (a) Uniaxial compressive strength as a function of tensile strength for rocks from La Soufrière de Guadeloupe, Chaos Crags, and Merapi volcano. (b) The ratio of compressive to tensile strength as a function of average connected porosity. (c) The ratio of compressive to tensile strength as a function of alteration (the weight percentage of secondary minerals). Data available in Table 4.

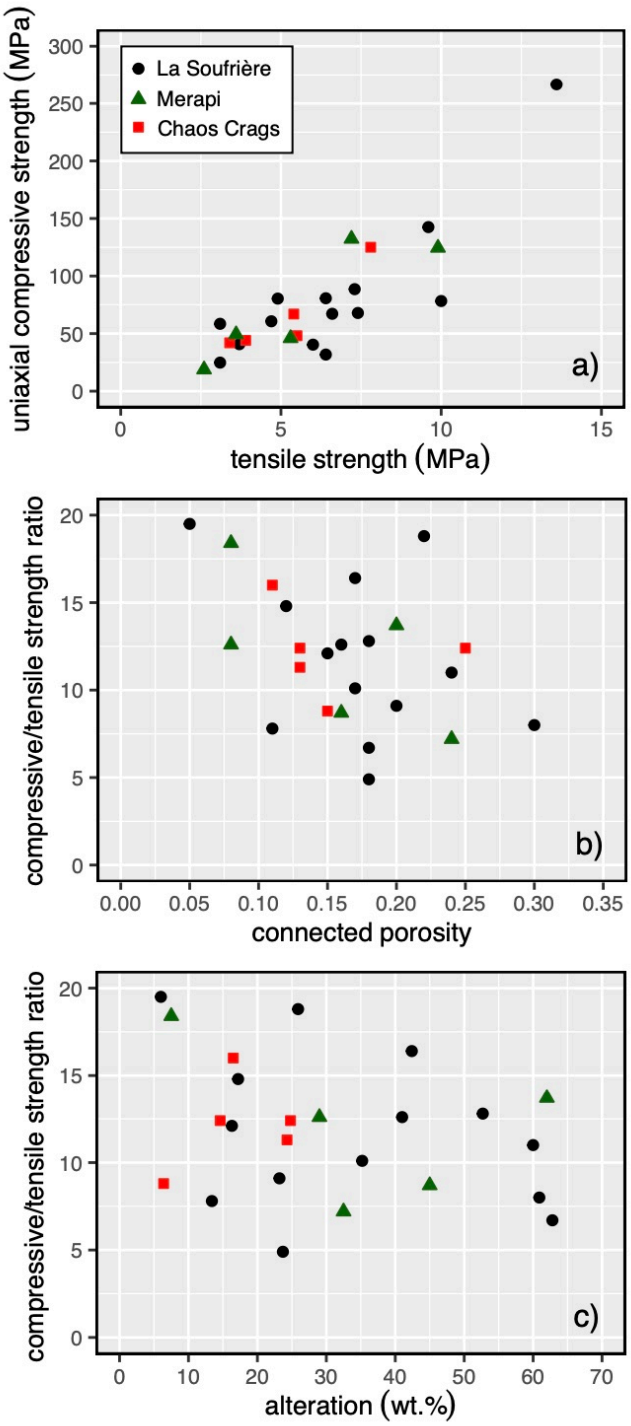

731 **Fig. 12.** Discrete element method models using Particle Flow Code 2D to show the influence
732 of homogeneously altered host rock in response to pressurisation of a magma-filled dyke. Host
733 rock properties correspond to the following scenarios: (a) weak hydrothermally altered host-
734 rock, (b) unaltered intact host-rock, (c) strong hydrothermally altered host-rock. The
735 mechanical properties for these scenarios can be found in Table 5. Red particles show unbonded
736 fluid magma; grey particles show bonded host-rock; and black lines show bond breakage,
737 indicating microcracking of the host-rock and damage accumulation.

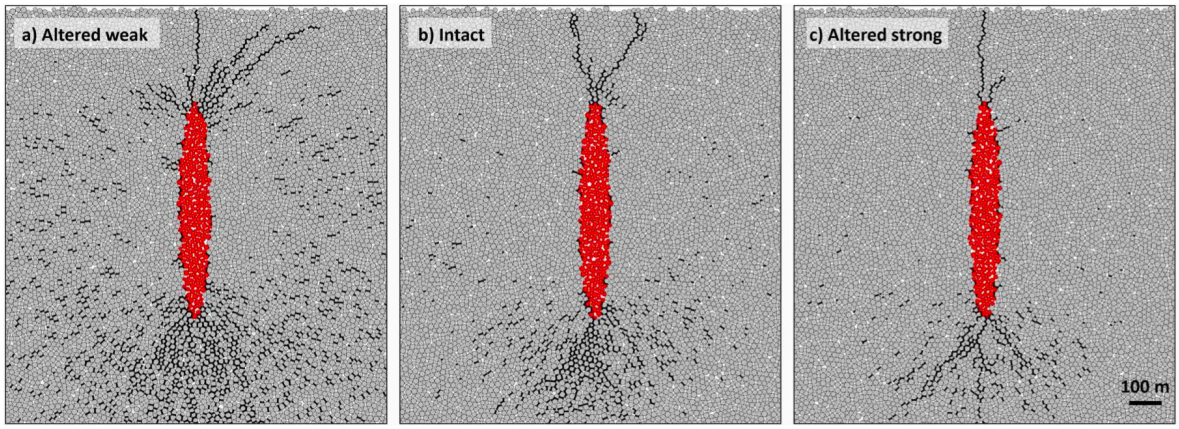

738

739

740 **Fig. 13.** Discrete element method models using Particle Flow Code 2D to show the influence
741 of homogeneously altered host rock in response to pressurisation of a magma-filled dyke. Host
742 rock properties correspond to the following scenarios: (a) low UCS/UTS ratio = 5, (b)
743 intermediate UCS/UTS ratio = 10 (equivalent to the intact properties in Fig. 12), (c) high
744 UCS/UTS ratio = 20. The mechanical properties for these scenarios can be found in Table 6.
745 Red particles show unbonded fluid magma; grey particles show bonded host-rock; and black
746 lines show bond breakage, indicating microcracking of the host-rock and damage accumulation.

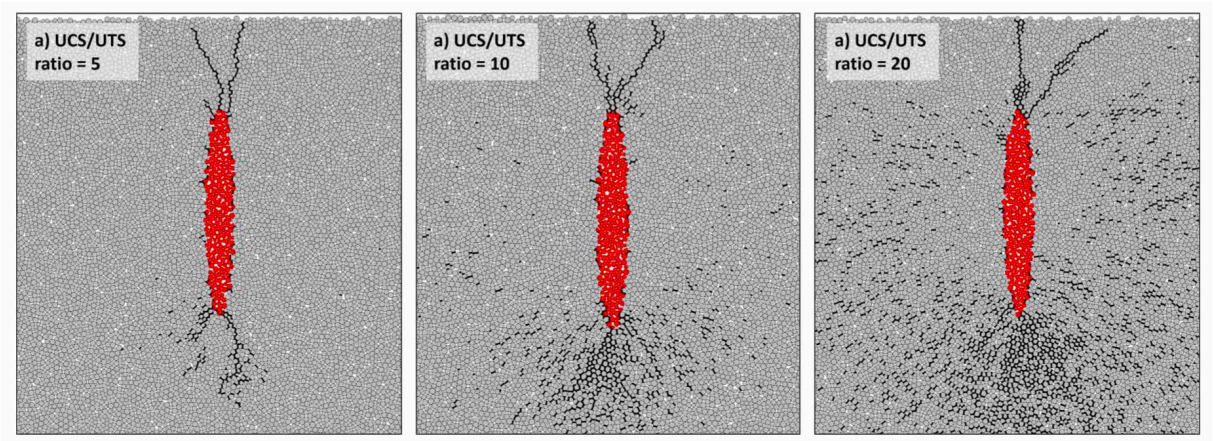

747

748

Tables

Table 1. Mineral contents, measured by X-ray powder diffraction and refined using Raman spectroscopy and optical microscopy, of the 15 blocks from La Soufrière de Guadeloupe (sampling locations shown in Fig. 1a), the five blocks from Chaos Crags (sampling locations shown in Fig. 1b), and the five blocks from Merapi volcano (sampling location shown in Fig. 1c). Values in wt%. Data from Heap et al. (2019, 2021a, 2022). Pl – plagioclase, Kfs – K-feldspar, Cpx – clinopyroxene, Opx – orthopyroxene, Mag – magnetite, Bt – biotite, Hbl – hornblende, Qtz – quartz, Crs – cristobalite, Trd – tridymite, O-A – opal-A, AP – amorphous phases, Hem – hematite, Py – pyrite, Alu – alunite, Na-Alu – Na-alunite, Gp – gypsum, Kln – kaolinite, Smc – smectite, Tlc – talc. Unless otherwise stated, the relative errors in the quantification are 5–10% (Heap et al., 2021a, 2022).

	Pl	Kfs	Cpx	Opx	Mag	Bt	Hbl	Qtz	Crs	Trd	O-A	AP	Hem	Py	Alu	Na-Alu	Gp	Kln	Smc	Tlc
H2A	56.7	-	8.7	10.8	0.7	-	-	1.0	11.3	-	-	-	-	3.5	-	1.4	-	6.0	-	-
H3	46.6	-	5.6	11.8	0.8	-	-	0.6	10.6	-	-	-	-	3.8	-	2.8	-	17.4	-	-
H4A	23.3	-	4.9	11.8	-	-	-	0.6	11.8	-	-	-	-	2.3	-	1.3	0.7	43.3	-	-
H5A	41.3	-	5.2	11.1	-	-	-	0.5	13.0	-	-	-	-	-	-	5.4	-	23.5	-	-
H6	30.0	-	6.4	10.8	-	-	-	0.5	11.1	-	-	-	-	-	-	5.1	-	36.0	-	-
H14	60.7	-	6.3	8.6	0.8	-	-	1.7	13.5	-	-	-	3.4	-	-	5.1	-	< 1	-	-
H15	22.5	-	7.3	9.2	-	-	-	0.7	10.2	-	-	-	0.7	-	-	15.0	-	34.3	-	-
H19	22.0	-	5.0	10.2	-	-	-	1.7	9.5	-	30.0	-	2.4	-	-	14.2	-	2.0	-	-
H21	24.2	-	12.4	19.3	3.1	-	-	0.2	11.7	-	-	-	-	0.4	-	0.5	1.2	2.0	-	-
H22	59.5	-	8.9	13.6	0.8	-	-	0.6	10.6	-	-	-	-	3.1	-	-	-	< 1	-	2.9
H29	62.4	-	7.8	11.2	2.7	-	-	0.4	12.4	-	10.0	-	3.1	-	-	-	-	-	-	-
H30	8.9	-	2.5	3.3	-	-	-	0.9	9.0	-	10.0	-	4.3	-	-	25.6	-	35.6	-	-
H32	64.4	-	9.5	15.1	4.9	-	-	0.3	5.7	-	-	-	-	-	-	-	-	-	-	-
WP 1285	64.7	-	5.2	13.2	3.5	-	-	0.2	-	13.2	-	-	-	-	-	-	-	-	-	-
WP 1317	61.6	-	5.9	15.6	0.7	-	-	0.7	-	13.2	-	-	-	-	2.4	-	-	-	-	-
CCC	52.6	16.8	2.3	-	0.3	2.5	1.0	17.8	5.2	-	-	-	1.2	-	-	-	-	-	-	-
CC3	47.1	7.0	6.5	13.2	-	-	-	1.4	-	-	-	23.8	1.0	-	-	-	-	-	-	-
CC4 A	36.3	14.6	1.7	-	0.6	3.1	1.7	25.4	9.8	-	-	-	0.6	-	-	-	-	4.8	1.3	-
CC4 B	42.9	16.7	2.2	-	0.5	3.5	1.8	17.8	8.7	-	-	-	0.8	-	-	-	-	4.2	0.9	-
CC10	58.9	10.5	-	-	1.0	0.2	1.0	4.0	22.2	-	-	-	2.1	-	-	-	-	-	-	-
M-U	54 ± 3	19 ± 3	16 ± 2		3 ± 0.5	-	-	1 ± 0.5	6 ± 0.5	-	-	-	0.5 ± 0.5	-	-	-	-	-	-	-
M-SA1	47 ± 3	9 ± 3	13 ± 2		2 ± 0.5	-	-	1.5 ± 0.5	-	-	-	24 ± 4	2 ± 0.5	-	-	1 ± 0.5	0.5 ± 0.5	-	-	-
M-SA2	38 ± 3	13 ± 3	14 ± 2		2.5 ± 0.5	-	-	0.5 ± 0.5	-	-	-	19 ± 4	0.5 ± 0.5	-	-	8.5 ± 2	5 ± 0.5	-	-	-
M-HA1	38 ± 3	6 ± 3	11 ± 2		< 1 ± 0.5	-	-	1 ± 0.5	-	-	-	25 ± 4	3 ± 0.5	-	-	11 ± 2	5 ± 0.5	-	-	-
M-HA2	19 ± 3	10 ± 3	8 ± 2		< 1 ± 0.5	-	-	0.5 ± 0.5	2.5 ± 0.5	-	-	28 ± 4	1 ± 0.5	-	-	24 ± 2	6 ± 0.5	-	-	-

763 **Table 2.** Summary of the experimental data collected for this study (*data from Heap et al.,
764 2021c). Experimental errors for the measurements of porosity and tensile strength are < 1%.
765 Relative errors for the weight percentages are 5–10%.
766

Volcano	Sample	Connected porosity	Weight percentage of secondary minerals	Indirect tensile strength (MPa)
La Soufrière	H2A_T1	0.16	23.2	8.8
La Soufrière	H2A_T2	0.19	23.2	7.2
La Soufrière	H2A_T3	0.21	23.2	5.7
La Soufrière	H2A_T4	0.17	23.2	7.5
La Soufrière	H2A_T5	0.16	23.2	8.0
La Soufrière	H3_T1	0.20	35.2	6.5
La Soufrière	H3_T2	0.15	35.2	8.3
La Soufrière	H3_T3	0.17	35.2	5.8
La Soufrière	H3_T4	0.21	35.2	6.0
La Soufrière	H4A_T1	0.27	60	3.6
La Soufrière	H4A_T2	0.30	60	2.2
La Soufrière	H4A_T3	0.24	60	3.5
La Soufrière	H4A_T4	0.19	60	5.5
La Soufrière	H5A_T1	0.18	42.4	4.3
La Soufrière	H5A_T2	0.20	42.4	5.5
La Soufrière	H6_T1	0.20	52.7	5.5
La Soufrière	H6_T2	0.20	52.7	5.3
La Soufrière	H6_T3	0.20	52.7	3.1
La Soufrière	H6_T4	0.22	52.7	4.9
La Soufrière	H14_T1	0.16	23.7	6.9
La Soufrière	H14_T2	0.16	23.7	6.0
La Soufrière	H15_T1	0.32	60.9	2.5
La Soufrière	H15_T2	0.30	60.9	3.7
La Soufrière	H19_T1	0.18	62.8	5.2
La Soufrière	H19_T2	0.17	62.8	6.6
La Soufrière	H19_T3	0.18	62.8	6.7
La Soufrière	H19_T4	0.19	62.8	5.6
La Soufrière	H21_T1	0.18	41	7.4
La Soufrière	H21_T2	0.20	41	6.0
La Soufrière	H21_T3	0.21	41	6.3
La Soufrière	H21_T4	0.19	41	6.5
La Soufrière	H21_T5	0.18	41	5.8

La Soufrière	H22_T1	0.14	17.2	8.6
La Soufrière	H22_T2	0.13	17.2	9.0
La Soufrière	H22_T3	0.14	17.2	8.7
La Soufrière	H22_T4	0.12	17.2	10.6
La Soufrière	H22_T5	0.13	17.2	11.1
La Soufrière	H29_T1	0.27	25.9	3.4
La Soufrière	H29_T2	0.28	25.9	3.6
La Soufrière	H29_T3	0.33	25.9	0.9
La Soufrière	H29_T4	0.27	25.9	3.8
La Soufrière	H30_T1	0.28	45.8	4.6
La Soufrière	H32_T1	0.05	6	15.6
La Soufrière	H32_T2	0.05	6	13.8
La Soufrière	H32_T3	0.05	6	12.6
La Soufrière	H32_T4	0.05	6	12.7
La Soufrière	WP1285_T1	0.11	13.4	10.4
La Soufrière	WP1285_T2	0.08	13.4	10.6
La Soufrière	WP1285_T3	0.10	13.4	10.7
La Soufrière	WP1285_T4	0.11	13.4	8.9
La Soufrière	WP1285_T5	0.10	13.4	9.6
La Soufrière	WP1317_T1	0.15	16.3	6.5
La Soufrière	WP1317_T2	0.16	16.3	6.4
La Soufrière	WP1317_T3	0.15	16.3	7.5
La Soufrière	WP1317_T4	0.14	16.3	8.8
Chaos Crags*	CCC	0.14	6.4	5.8
Chaos Crags*	CCC	0.14	6.4	5.1
Chaos Crags	CC3_T1	0.29	24.8	4.4
Chaos Crags	CC3_T2	0.26	24.8	3.5
Chaos Crags	CC3_T3	0.23	24.8	5.2
Chaos Crags	CC3_T4	0.21	24.8	7.0
Chaos Crags	CC3_T5	0.20	24.8	6.6
Chaos Crags	CC4A_T1	0.09	16.5	7.8
Chaos Crags	CC4A_T2	0.08	16.5	8.3
Chaos Crags	CC4A_T3	0.08	16.5	7.9
Chaos Crags	CC4A_T4	0.08	16.5	7.1
Chaos Crags	CC4A_T5	0.08	16.5	7.6
Chaos Crags	CC4B_T1	0.16	14.6	3.0
Chaos Crags	CC4B_T2	0.14	14.6	3.4
Chaos Crags	CC4B_T3	0.16	14.6	4.4
Chaos Crags	CC4B_T4	0.15	14.6	3.1
Chaos Crags	CC10_T1	0.12	24.3	4.9
Chaos Crags	CC10_T2	0.16	24.3	3.7
Chaos Crags	CC10_T3	0.13	24.3	4.1

Chaos Crags	CC10_T4	0.15	24.3	2.7
Merapi*	MU	0.08	7.5	7.4
Merapi*	MU	0.09	7.5	7.0
Merapi*	MSA1	0.22	32.5	3.0
Merapi*	MSA1	0.25	32.5	2.1
Merapi*	MSA2	0.09	29.0	9.7
Merapi*	MSA2	0.09	29.0	10.1
Merapi*	MHA1	0.18	45.0	6.0
Merapi*	MHA1	0.21	45.0	4.6
Merapi	MHA2	0.17	62.0	3.1
Merapi	MHA2	0.22	62.0	4.0

767

768 **Table 3.** Best-fit values for the effective characteristic tensile stress, T_0, for the compiled dataset
769 in Heap et al. (2021c) and for the variably altered andesites from La Soufrière de Guadeloupe
770 (data from this study). Note: the goodness of fit values quoted in Heap et al. (2021c) were the
771 linear residual ratios, rather than the formal R^2 values shown here.
772

Model	**Best-fit T_0 for the compiled dataset (from Heap et al., 2021c) in MPa**	**Goodness of fit (from Heap et al., 2021c)***	**Best-fit T_0 for the variably altered andesites from La Soufrière de Guadeloupe**	**Goodness of fit for the La Soufrière de Guadeloupe dataset***
Spieler et al. (2004) Eq. 2a	0.43	0.26	0.90	0.6414
McBirney and Murase (1970) Eq. 2b	0.51	0.13	0.98	0.4870
Zhang (1999) Eq. 2c	3.14	0.57	5.84	0.4724
Alidibirov (1994) Eq. 2d	2.00	0.44	4.12	0.7068
Koyaguchi et al. (2008) Eq. 2d	0.76	0.45	1.48	0.4743
Koyaguchi et al. (2008) Eq. 2e	0.77	0.13	1.67	0.7211

773 * The goodness of fit R^2 is computed in the standard way, but using the $\log(T_m)$, $\log(T_p)$, and
774 the mean of $\log(T_m)$, where T_m is the measured tensile strength and T_p is the predicted tensile
775 strength.

Table 4. Average ratios of compressive to tensile strength for the rocks from La Soufrière de Guadeloupe, Chaos Crags, and Merapi volcano. Also shown are the average porosities, alteration (percentage of secondary minerals), and the average uniaxial compressive and tensile strength. Data for the uniaxial compressive strength of the rocks from La Soufrière de Guadeloupe, Chaos Crags, and Merapi volcano are published in Heap et al. (2021a), Heap et al. (2021b), and Darmawan et al. (2022). Experimental errors for the measurements of porosity, tensile strength, and uniaxial compressive strength are < 1%. Relative errors for the weight percentages are in the order of 5–10%. Standard deviations are provided for the average connected porosities and average compressive strengths. Data are two few to provide standard deviations for the average tensile strengths.

Volcano	Block	Average connected porosity	Weight percentage of secondary minerals	Average compressive strength (MPa)	Average indirect tensile strength (MPa)	Ratio of compressive to tensile strength
La Soufrière	2A	0.20 ± 0.04	23.2	67.9 ± 8.1	7.4	9.1
La Soufrière	2B	0.42 ± 0.02	74.6	6.9 ± 1.6	-	-
La Soufrière	3	0.17 ± 0.02	35.2	67.2 ± 4.9	6.6	10.1
La Soufrière	4A	0.24 ± 0.02	60.0	40.8 ± 2.5	3.7	11.0
La Soufrière	5A	0.17 ± 0.02	42.4	80.4 ± 8.4	4.9	16.4
La Soufrière	6	0.18 ± 0.01	52.7	60.7 ± 6.3	4.7	12.8
La Soufrière	14	0.18 ± 0.02	23.7	31.8 ± 19.5	6.4	4.9
La Soufrière	15	0.30 ± 0.03	60.9	24.8 ± 2.2	3.1	8.0
La Soufrière	18	0.12 ± 0.01	15.2	99.3 ± 9.2	-	-

La Soufrière	19	0.18 ± 0.03	62.8	40.4 ± 4.8	6.0	6.7
La Soufrière	20	0.37 ± 0.02	45.0	4.7 ± 0.9	-	-
La Soufrière	21	0.16 ± 0.01	41.0	80.7 ± 10.7	6.4	12.6
La Soufrière	22	0.12 ± 0.00	17.2	142.5 ± 6.2	9.6	14.8
La Soufrière	25	0.16 ± 0.03	45.8	92.4 ± 7.1	-	-
La Soufrière	29	0.22 ± 0.03	25.9	58.5 ± 9.8	3.1	18.8
La Soufrière	30	0.25 ± 0.11	85.4	-	4.6	-
La Soufrière	32	0.05 ± 0.00	6.0	266.6 ± 8.7	13.6	19.5
La Soufrière	WP1285	0.11 ± 0.02	13.4	78.3 ± 9.4	10.0	7.8
La Soufrière	WP1317	0.15 ± 0.02	16.3	88.6 ± 13.9	7.3	12.1
Chaos Crags	CCC	0.15 ± 0.00	6.4	48.2 ± 2.6	5.5	8.8
Chaos Crags	CC3	0.25 ± 0.02	24.8	67.0 ± 1.3	5.4	12.4
Chaos Crags	CC4A	0.11 ± 0.03	16.5	125.0 ± 8.0	7.8	16.0
Chaos Crags	CC4B	0.13 ± 0.01	14.6	42.0 ± 5.0	3.4	12.4
Chaos Crags	CC10	0.13 ± 0.01	24.3	44.1 ± 4.6	3.9	11.3
Merapi	M-U	0.08 ± 0.00	7.5	132.3 ± 11.3	7.2	18.4
Merapi	M-SA1	0.24 ± 0.02	32.5	18.8 ± 6.9	2.6	7.2
Merapi	M-SA2	0.08 ± 0.00	29.0	124.5 ± 13.1	9.9	12.6
Merapi	M-HA1	0.16 ± 0.01	45.0	46.0 ± 6.9	5.3	8.7
Merapi	M-HA2	0.20 ± 0.03	62.0	49.3 ± 21.5	3.6	13.7

787

788 **Table 5.** Target bulk properties (Young's modulus, uniaxial compressive strength (UCS),
789 uniaxial tensile strength (UTS), and UCS/UTS ratio) for each of the three strength scenarios
790 considered. Target bulk properties for each scenario are guided by the laboratory data presented
791 here. Resultant bulk properties are achieved by an iterative model calibration process within
792 Particle Flow Code 2D. Averages (plus/minus one standard deviation) are given from 10
793 simulated tests, each with different random particle packing arrangements to account for the
794 variation in packing that occurs in the large-scale models.
795

	Strength scenario	**Young's modulus (GPa)**	**Uniaxial compressive strength (MPa)**	**Tensile strength (MPa)**	**UCS/UTS ratio**
Target bulk properties	Intact	30	100	10	10
	Altered weak	25	50	5	10
	Altered strong	35	150	15	10
Resultant bulk properties	Intact	30.0 ± 0.2	99.5 ± 5.7	10.2 ± 0.9	9.9 ± 1.3
	Altered weak	24.9 ± 0.2	49.9 ± 3.1	4.8 ± 0.4	10.6 ± 1.4
	Altered strong	35.2 ± 0.3	150.6 ± 8.1	15.3 ± 1.4	10.0 ± 1.2

796

797 **Table 6.** Target bulk properties (Young's modulus, uniaxial compressive strength (UCS),
798 uniaxial tensile strength (UTS), and UCS/UTS ratio) for each of the three UCS/UTS ratio
799 scenarios considered. Target bulk properties for each scenario are guided by the laboratory data
800 presented here. Resultant bulk properties are achieved by an iterative model calibration process
801 within Particle Flow Code 2D. Averages (plus/minus one standard deviation) are given from
802 10 simulated tests, each with different random particle packing arrangements to account for the
803 variation in packing that occurs in the large-scale models.
804

	Strength scenario	**Young's modulus (GPa)**	**Uniaxial compressive strength (MPa)**	**Tensile strength (MPa)**	**UCS/UTS ratio**
Target bulk properties	Intermediate UCS/UTS ratio	30	100	10	10
	Low UCS/UTS ratio	30	100	20	5
	High UCS/UTS ratio	30	100	5	20
Resultant bulk properties	Intermediate UCS/UTS ratio	30.0 ± 0.2	99.5 ± 5.7	10.2 ± 0.9	9.9 ± 1.3
	Low UCS/UTS ratio	30.2 ± 0.2	100.2 ± 3.1	19.7 ± 1.8	5.2 ± 0.6
	High UCS/UTS ratio	30.3 ± 0.2	99.5 ± 9.3	5.1 ± 0.5	19.6 ± 2.9

805
806

References

Acocella, V. (2021). Volcano-Tectonic Processes. Springer Nature.

Alidibirov, M. A. (1994). A model for viscous magma fragmentation during volcanic blasts. Bulletin of Volcanology, 56(6), 459-465.

Aldeeky, H., & Al Hattamleh, O. (2018). Prediction of engineering properties of basalt rock in Jordan using ultrasonic pulse velocity test. Geotechnical and Geological Engineering, 36(6), 3511-3525.

Arnórsson, S. (1995). Geothermal systems in Iceland: structure and conceptual models—I. High-temperature areas. Geothermics, 24(5-6), 561-602.

Ball, J. L., Stauffer, P. H., Calder, E. S., & Valentine, G. A. (2015). The hydrothermal alteration of cooling lava domes. Bulletin of Volcanology, 77(12), 1-16.

Ball, J. L., Taron, J., Reid, M. E., Hurwitz, S., Finn, C., & Bedrosian, P. (2018). Combining multiphase groundwater flow and slope stability models to assess stratovolcano flank collapse in the Cascade Range. Journal of Geophysical Research: Solid Earth, 123(4), 2787-2805.

Bergmann, J., Friedel, P., & Kleeberg, R. (1998). BGMN—a new fundamental parameters based Rietveld program for laboratory X-ray sources, its use in quantitative analysis and structure investigations. CPD Newsletter, 20(5).

Boudon, G., Villemant, B., Komorowski, J. C., Ildefonse, P., & Semet, M. P. (1998). The hydrothermal system at Soufriere Hills Volcano, Montserrat (West Indies): Characterization and role in the on-going eruption. Geophysical Research Letters, 25(19), 3693-3696.

Browne, P. R. L. (1978). Hydrothermal alteration in active geothermal fields. Annual review of earth and planetary sciences, 6(1), 229-248.

Byrdina, S., Friedel, S., Vandemeulebrouck, J., Budi-Santoso, A., Suryanto, W., Rizal, M. H., & Winata, E. (2017). Geophysical image of the hydrothermal system of Merapi volcano. Journal of Volcanology and Geothermal Research, 329, 30-40.

Cai, M. (2010). Practical estimates of tensile strength and Hoek–Brown strength parameter mi of brittle rocks. Rock Mechanics and Rock Engineering, 43(2), 167-184.

Cant, J. L., Siratovich, P. A., Cole, J. W., Villeneuve, M. C., & Kennedy, B. M. (2018). Matrix permeability of reservoir rocks, Ngatamariki geothermal field, Taupo Volcanic Zone, New Zealand. Geothermal Energy, 6(1), 1-28.

Cecchi, E., de Vries, B. V. W., & Lavest, J. M. (2004). Flank spreading and collapse of weak-cored volcanoes. Bulletin of Volcanology, 67(1), 72-91.

Chen, T. C., Yeung, M. R., & Mori, N. (2004). Effect of water saturation on deterioration of welded tuff due to freeze-thaw action. Cold Regions Science and Technology, 38(2-3), 127-136.

Chen, T., Cheng, S., Fang, Q., & Zhou, C. (2017). Numerical modeling of shallow magma intrusions with finite element method. Journal of Volcanology and Geothermal Research, 333, 53-65.

Clynne, M. A., & Muffler, L. P. (2017). Geologic field-trip guide to the Lassen segment of the Cascades Arc, northern California (No. 2017-5022-K2). US Geological Survey.

Darmawan, H., Troll, V. R., Walter, T. R., Deegan, F. M., Geiger, H., Heap, M. J., Seraphine, N., Harris, C., Humaida, H., & Müller, D. (2022). Hidden mechanical weaknesses within lava domes provided by buried high-porosity hydrothermal alteration zones. Scientific Reports, 12, 3202.

Day, S. J. (1996). Hydrothermal pore fluid pressure and the stability of porous, permeable volcanoes. Geological Society, London, Special Publications, 110(1), 77-93.

de Moor, J. M., Stix, J., Avard, G., Muller, C., Corrales, E., Diaz, J. A., ... & Fischer, T. P. (2019). Insights on hydrothermal-magmatic interactions and eruptive processes at Poás Volcano (Costa Rica) from high-frequency gas monitoring and drone measurements. Geophysical Research Letters, 46(3), 1293-1302.

del Potro, R., & Hürlimann, M. (2009). The decrease in the shear strength of volcanic materials with argillic hydrothermal alteration, insights from the summit region of Teide stratovolcano, Tenerife. Engineering Geology, 104(1-2), 135-143.

Edmonds, M., Oppenheimer, C., Pyle, D. M., Herd, R. A., & Thompson, G. (2003). SO2 emissions from Soufrière Hills Volcano and their relationship to conduit permeability, hydrothermal interaction and degassing regime. Journal of Volcanology and Geothermal Research, 124(1-2), 23-43.

Ersoy, A., & Atici, U. (2007). Correlation of P and S-Waves with Cutting Specific Energy and Dominant Properties of Volcanic and Carbonate Rocks. Rock Mechanics and Rock Engineering, 40(5), 491-504.

Farquharson, J. I., Wild, B., Kushnir, A. R., Heap, M. J., Baud, P., & Kennedy, B. (2019). Acid-induced dissolution of andesite: evolution of permeability and strength. Journal of Geophysical Research: Solid Earth, 124(1), 257-273.

Fener, M., & Ince, I. (2015). Effects of the freeze–thaw (F–T) cycle on the andesitic rocks (Sille-Konya/Turkey) used in construction building. Journal of African Earth Sciences, 109, 96-106.

Folch, A., & Martı, J. (2004). Geometrical and mechanical constraints on the formation of ring-fault calderas. Earth and Planetary Science Letters, 221(1-4), 215-225.

Friðleifsson, G. Ó., & Elders, W. A. (2005). The Iceland Deep Drilling Project: a search for deep unconventional geothermal resources. Geothermics, 34(3), 269-285.

Frolova, J., Ladygin, V., Rychagov, S., & Zukhubaya, D. (2014). Effects of hydrothermal alterations on physical and mechanical properties of rocks in the Kuril–Kamchatka island arc. Engineering Geology, 183, 80-95.

Ghorbani, A., Revil, A., Coperey, A., Ahmed, A. S., Roque, S., Heap, M. J., ... & Viveiros, F. (2018). Complex conductivity of volcanic rocks and the geophysical mapping of alteration in volcanoes. Journal of Volcanology and Geothermal Research, 357, 106-127.

Goto, Y., Nakada, S., Kurokawa, M., Shimano, T., Sugimoto, T., Sakuma, S., ... & Uto, K. (2008). Character and origin of lithofacies in the conduit of Unzen volcano, Japan. Journal of Volcanology and Geothermal Research, 175(1-2), 45-59.

Graue, B., Siegesmund, S., & Middendorf, B. (2011). Quality assessment of replacement stones for the Cologne Cathedral: mineralogical and petrophysical requirements. Environmental Earth Sciences, 63(7-8), 1799-1822.

Griffiths, L., Lengliné, O., Heap, M. J., Baud, P., & Schmittbuhl, J. (2018). Thermal cracking in Westerly Granite monitored using direct wave velocity, coda wave interferometry, and acoustic emissions. Journal of Geophysical Research: Solid Earth, 123(3), 2246-2261.

Gudmundsson, A. (2006). How local stresses control magma-chamber ruptures, dyke injections, and eruptions in composite volcanoes. Earth-Science Reviews, 79(1-2), 1-31.

Gudmundsson, A. (2020). Volcanotectonics: Understanding the structure, deformation and dynamics of volcanoes. Cambridge University Press.

Gupta, A. S., & Rao, K. S. (2000). Weathering effects on the strength and deformational behaviour of crystalline rocks under uniaxial compression state. Engineering Geology, 56(3-4), 257-274.

Harnett, C. E., Thomas, M. E., Purvance, M. D., & Neuberg, J. (2018). Using a discrete element approach to model lava dome emplacement and collapse. Journal of Volcanology and Geothermal Research, 359, 68-77.

Harnett, C. E., Kendrick, J. E., Lamur, A., Thomas, M. E., Stinton, A., Wallace, P. A., ... & Lavallée, Y. (2019). Evolution of mechanical properties of lava dome rocks across the 1995–2010 eruption of Soufrière Hills volcano, Montserrat. Frontiers in Earth Science, 7, 7.

Harnett, C. E., Heap, M. J., & Thomas, M. E. (2020). A toolbox for identifying the expression of dome-forming volcanism on exoplanets. Planetary and Space Science, 180, 104762.

Harnett, C. E., & Heap, M. J. (2021). Mechanical and topographic factors influencing lava dome growth and collapse. Journal of Volcanology and Geothermal Research, 420, 107398.

Hashiba, K., & Fukui, K. (2015). Effect of water on the deformation and failure of rock in uniaxial tension. Rock Mechanics and Rock Engineering, 48(5), 1751-1761.

Heap, M. J., Lavallée, Y., Laumann, A., Hess, K. U., Meredith, P. G., & Dingwell, D. B. (2012). How tough is tuff in the event of fire? Geology, 40(4), 311-314.

Heap, M. J., Xu, T., & Chen, C. F. (2014). The influence of porosity and vesicle size on the brittle strength of volcanic rocks and magma. Bulletin of Volcanology, 76(9), 1-15.

Heap, M. J., Wadsworth, F. B., Xu, T., & Chen, C. F. (2016). The strength of heterogeneous volcanic rocks: a 2D approximation. Journal of Volcanology and Geothermal Research, 319, 1-11.

Heap, M. J., Kennedy, B. M., Farquharson, J. I., Ashworth, J., Mayer, K., Letham-Brake, M., ... & Dingwell, D. B. (2017). A multidisciplinary approach to quantify the permeability of the Whakaari/White Island volcanic hydrothermal system (Taupo Volcanic Zone, New Zealand). Journal of Volcanology and Geothermal Research, 332, 88-108.

Heap, M. J., Troll, V. R., Kushnir, A. R., Gilg, H. A., Collinson, A. S., Deegan, F. M., ... & Walter, T. R. (2019). Hydrothermal alteration of andesitic lava domes can lead to explosive volcanic behaviour. Nature Communications, 10(1), 1-10.

Heap, M. J., Gravley, D. M., Kennedy, B. M., Gilg, H. A., Bertolett, E., & Barker, S. L. (2020). Quantifying the role of hydrothermal alteration in creating geothermal and epithermal mineral resources: the Ohakuri ignimbrite (Taupō Volcanic Zone, New Zealand). Journal of Volcanology and Geothermal Research, 390, 106703.

Heap, M. J., Baumann, T. S., Rosas-Carbajal, M., Komorowski, J. C., Gilg, H. A., Villeneuve, M., ... & Reuschlé, T. (2021a). Alteration-Induced Volcano Instability at La Soufrière de

Guadeloupe (Eastern Caribbean). Journal of Geophysical Research: Solid Earth, 126(8), e2021JB022514.
Heap, M. J., Baumann, T., Gilg, H. A., Kolzenburg, S., Ryan, A. G., Villeneuve, M., ... & Clynne, M. A. (2021b). Hydrothermal alteration can result in pore pressurization and volcano instability. Geology, 49(11), 1348-1352.
Heap, M. J., Wadsworth, F. B., Heng, Z., Xu, T., Griffiths, L., Velasco, A. A., ... & Deegan, F. M. (2021c). The tensile strength of volcanic rocks: Experiments and models. Journal of Volcanology and Geothermal Research, 418, 107348.
Heap, M. J., Jessop, D. E., Wadsworth, F. B., Rosas-Carbajal, M., Komorowski, J. C., Gilg, H. A., ... & Moretti, R. (2022). The thermal properties of hydrothermally altered andesites from La Soufrière de Guadeloupe (Eastern Caribbean). Journal of Volcanology and Geothermal Research, 421, 107444.
Heap, M. J., & Violay, M. E. (2021). The mechanical behaviour and failure modes of volcanic rocks: a review. Bulletin of Volcanology, 83(5), 1-47.
Heiken, G., & Eichelberger, J. C. (1980). Eruptions at Chaos Crags, Lassen Volcanic National Park, California. Journal of Volcanology and Geothermal Research, 7(3-4), 443-481.
Holohan, E. P., Schöpfer, M. P. J., & Walsh, J. J. (2011). Mechanical and geometric controls on the structural evolution of pit crater and caldera subsidence. Journal of Geophysical Research: Solid Earth, 116(B7).
Holohan, E. P., Walter, T. R., Schöpfer, M. P., Walsh, J. J., van Wyk de Vries, B., & Troll, V. R. (2013). Origins of oblique-slip faulting during caldera subsidence. Journal of Geophysical Research: Solid Earth, 118(4), 1778-1794.
Holohan, E. P., Schöpfer, M. P. J., & Walsh, J. J. (2015). Stress evolution during caldera collapse. Earth and Planetary Science Letters, 421, 139-151.
Holohan, E. P., Sudhaus, H., Walter, T. R., Schöpfer, M. P., & Walsh, J. J. (2017). Effects of host-rock fracturing on elastic-deformation source models of volcano deflation. Scientific Reports, 7(1), 1-12.
Hornby, A. J., Lavallée, Y., Kendrick, J. E., De Angelis, S., Lamur, A., Lamb, O. D., ... & Chigna, G. (2019). Brittle-ductile deformation and tensile rupture of dome lava during inflation at Santiaguito, Guatemala. Journal of Geophysical Research: Solid Earth, 124(10), 10107-10131.
Kahraman, S., & Yeken, T. (2010). Electrical resistivity measurement to predict uniaxial compressive and tensile strength of igneous rocks. Bulletin of Materials Science, 33(6), 731-735.
Kanakiya, S., Adam, L., Rowe, M. C., Lindsay, J. M., & Esteban, L. (2021). The role of tuffs in sealing volcanic conduits. Geophysical Research Letters, e2021GL095175.
Karakuş, A., & Akatay, M. (2013). Determination of basic physical and mechanical properties of basaltic rocks from P-wave velocity. Nondestructive Testing and Evaluation, 28(4), 342-353.
Kendrick, J. E., Schaefer, L. N., Schauroth, J., Bell, A. F., Lamb, O. D., Lamur, A., ... & Kennedy, B. M. (2021). Physical and mechanical rock properties of a heterogeneous volcano: the case of Mount Unzen, Japan. Solid Earth, 12(3), 633-664.
Kennedy, B. M., Farquhar, A., Hilderman, R., Villeneuve, M. C., Heap, M. J., Mordensky, S., ... & Reuschlé, T. (2020). Pressure controlled permeability in a conduit filled with

fractured hydrothermal breccia reconstructed from ballistics from Whakaari (White Island), New Zealand. Geosciences, 10(4), 138.
Kereszturi, G., Schaefer, L. N., Miller, C., & Mead, S. (2020). Hydrothermal alteration on composite volcanoes: mineralogy, hyperspectral imaging, and aeromagnetic study of Mt Ruapehu, New Zealand. Geochemistry, Geophysics, Geosystems, 21(9), e2020GC009270.
Kilburn, C. R. (2018). Forecasting volcanic eruptions: Beyond the failure forecast method. Frontiers in Earth Science, 6, 133.
Kılıç, A., & Teymen, A. (2008). Determination of mechanical properties of rocks using simple methods. Bulletin of Engineering Geology and the Environment, 67(2), 237.
Komorowski J.-C., Boudon G., Semet, M., Beauducel, F., Anténor-Habazac, C., Bazin, S., Hammmouya. G. (2005). Guadeloupe. J. Lindsay, R. Robertson, J. Shepherd, S. Ali (Eds.), Volcanic Atlas of the Lesser Antilles, University of the French West Indies, Seismic Research Unit, 65-102.
Koyaguchi, T., Scheu, B., Mitani, N. K., & Melnik, O. (2008). A fragmentation criterion for highly viscous bubbly magmas estimated from shock tube experiments. Journal of Volcanology and Geothermal Research, 178(1), 58-71.
Lamb, O. D., De Angelis, S., Wall, R. J., Lamur, A., Varley, N. R., Reyes-Dávila, G., ... & Lavallée, Y. (2017). Seismic and experimental insights into eruption precursors at Volcán de Colima. Geophysical Research Letters, 44(12), 6092-6100.
Lavallée, Y., Varley, N. R., Alatorre-Ibargüengoitia, M. A., Hess, K. U., Kueppers, U., Mueller, S., ... & Dingwell, D. B. (2012). Magmatic architecture of dome-building eruptions at Volcán de Colima, Mexico. Bulletin of Volcanology, 74(1), 249-260.
Lévy, L., Gibert, B., Sigmundsson, F., Flóvenz, Ó. G., Hersir, G. P., Briole, P., & Pezard, P. A. (2018). The role of smectites in the electrical conductivity of active hydrothermal systems: electrical properties of core samples from Krafla volcano, Iceland. Geophysical Journal International, 215(3), 1558-1582.
Malik, A., Chakraborty, T., Rao, K. S., & Kumar, D. (2017). Experiments to determine static and dynamic tensile strength of deccan trap rocks, India. Procedia Engineering, 191, 946-953.
Marks, N., Schiffman, P., Zierenberg, R. A., Franzson, H., & Fridleifsson, G. Ó. (2010). Hydrothermal alteration in the Reykjanes geothermal system: Insights from Iceland deep drilling program well RN-17. Journal of Volcanology and Geothermal Research, 189(1-2), 172-190.
Marmoni, G. M., Martino, S., Heap, M. J., & Reuschlé, T. (2017). Gravitational slope-deformation of a resurgent caldera: New insights from the mechanical behaviour of Mt. Nuovo tuffs (Ischia Island, Italy). Journal of Volcanology and Geothermal Research, 345, 1-20.
Mayer, K., Scheu, B., Montanaro, C., Yilmaz, T. I., Isaia, R., Aßbichler, D., & Dingwell, D. B. (2016). Hydrothermal alteration of surficial rocks at Solfatara (Campi Flegrei): Petrophysical properties and implications for phreatic eruption processes. Journal of Volcanology and Geothermal Research, 320, 128-143.

Mayer, K., Scheu, B., Yilmaz, T. I., Montanaro, C., Gilg, H. A., Rott, S., ... & Dingwell, D. B. (2017). Phreatic activity and hydrothermal alteration in the Valley of Desolation, Dominica, Lesser Antilles. Bulletin of Volcanology, 79(12), 1-19.

McBirney, A. R., & Murase, T. (1970). Factors governing the formation of pyroclastic rocks. Bulletin Volcanologique, 34(2), 372-384.

McNamara, D. D., Sewell, S., Buscarlet, E., & Wallis, I. C. (2016). A review of the Rotokawa geothermal field, New Zealand. Geothermics, 59, 281-293.

Mick, E., Stix, J., de Moor, J. M., & Avard, G. (2021). Hydrothermal alteration and sealing at Turrialba volcano, Costa Rica, as a mechanism for phreatic eruption triggering. Journal of Volcanology and Geothermal Research, 107297.

Montanaro, C., Scheu, B., Mayer, K., Orsi, G., Moretti, R., Isaia, R., & Dingwell, D. B. (2016). Experimental investigations on the explosivity of steam-driven eruptions: A case study of Solfatara volcano (Campi Flegrei). Journal of Geophysical Research: Solid Earth, 121(11), 7996-8014.

Moon, K., & Yang, S. B. (2020). Cohesion and Internal Friction Angle Estimated from Brazilian Tensile Strength and Unconfined Compressive Strength of Volcanic Rocks in Jeju Island. Journal of the Korean Geotechnical Society, 36(2), 17-28.

Moretti, R., Komorowski, J. C., Ucciani, G., Moune, S., Jessop, D., de Chabalier, J. B., ... & Chaussidon, M. (2020). The 2018 unrest phase at La Soufrière of Guadeloupe (French West Indies) andesitic volcano: Scrutiny of a failed but prodromal phreatic eruption. Journal of Volcanology and Geothermal Research, 393, 106769.

Mordensky, S. P., Villeneuve, M. C., Kennedy, B. M., Heap, M. J., Gravley, D. M., Farquharson, J. I., & Reuschlé, T. (2018). Physical and mechanical property relationships of a shallow intrusion and volcanic host rock, Pinnacle Ridge, Mt. Ruapehu, New Zealand. Journal of Volcanology and Geothermal Research, 359, 1-20.

Mordensky, S. P., Heap, M. J., Kennedy, B. M., Gilg, H. A., Villeneuve, M. C., Farquharson, J. I., & Gravley, D. M. (2019). Influence of alteration on the mechanical behaviour and failure mode of andesite: implications for shallow seismicity and volcano monitoring. Bulletin of Volcanology, 81(8), 1-12.

Mueller, S., Scheu, B., Spieler, O., & Dingwell, D. B. (2008). Permeability control on magma fragmentation. Geology, 36(5), 399-402.

Mueller, D., Bredemeyer, S., Zorn, E., De Paolo, E., & Walter, T. R. (2021). Surveying fumarole sites and hydrothermal alteration by unoccupied aircraft systems (UAS) at the La Fossa cone, Vulcano Island (Italy). Journal of Volcanology and Geothermal Research, 413, 107208.

Nara, Y., Takada, M., Mori, D., Owada, H., Yoneda, T., & Kaneko, K. (2010). Subcritical crack growth and long-term strength in rock and cementitious material. International Journal of Fracture, 164(1), 57-71.

Nicolas, A., Lévy, L., Sissmann, O., Li, Z., Fortin, J., Gibert, B., & Sigmundsson, F. (2020). Influence of hydrothermal alteration on the elastic behaviour and failure of heat-treated andesite from Guadeloupe. Geophysical Journal International, 223(3), 2038-2053.

Opfergelt, S., Delmelle, P., Boivin, P., & Delvaux, B. (2006). The 1998 debris avalanche at Casita volcano, Nicaragua: Investigation of the role of hydrothermal smectite in promoting slope instability. Geophysical Research Letters, 33(15).

Peng, J., Wong, L. N. Y., & Teh, C. I. (2017). Influence of grain size heterogeneity on strength and microcracking behavior of crystalline rocks. Journal of Geophysical Research: Solid Earth, 122(2), 1054-1073.

Perras, M. A., & Diederichs, M. S. (2014). A review of the tensile strength of rock: concepts and testing. Geotechnical and geological engineering, 32(2), 525-546.

Pola, A., Crosta, G. B., Fusi, N., & Castellanza, R. (2014). General characterization of the mechanical behaviour of different volcanic rocks with respect to alteration. Engineering Geology, 169, 1-13.

Potyondy, D. (2016). Material-Modeling Support in PFC [via fistPkg23]. Technical Memorandum ICG7766-L, Itasca Consulting Group, Inc. Minneapolis, MN.

Potyondy, D. O. (2012, June). A flat-jointed bonded-particle material for hard rock. In 46th US Rock Mechanics/Geomechanics Symposium. OnePetro.

Potyondy, D. O., & Cundall, P. A. (2004). A bonded-particle model for rock. International Journal of Rock Mechanics and Mining Sciences, 41(8), 1329-1364.

Reid, M. E., Sisson, T. W., & Brien, D. L. (2001). Volcano collapse promoted by hydrothermal alteration and edifice shape, Mount Rainier, Washington. Geology, 29(9), 779-782.

Reid, M. E. (2004). Massive collapse of volcano edifices triggered by hydrothermal pressurization. Geology, 32(5), 373-376.

Roman, D. C., & Cashman, K. V. (2018). Top–down precursory volcanic seismicity: implications for 'stealth' magma ascent and long-term eruption forecasting. Frontiers in Earth Science, 6, 124.

Rosas-Carbajal, M., Komorowski, J. C., Nicollin, F., & Gibert, D. (2016). Volcano electrical tomography unveils edifice collapse hazard linked to hydrothermal system structure and dynamics. Scientific Reports, 6(1), 1-11.

Rowland, J. V., & Simmons, S. F. (2012). Hydrologic, magmatic, and tectonic controls on hydrothermal flow, Taupo Volcanic Zone, New Zealand: Implications for the formation of epithermal vein deposits. Economic Geology, 107(3), 427-457.

Ryan, A. G., Heap, M. J., Russell, J. K., Kennedy, L. A., & Clynne, M. A. (2020). Cyclic shear zone cataclasis and sintering during lava dome extrusion: Insights from Chaos Crags, Lassen Volcanic Center (USA). Journal of Volcanology and Geothermal Research, 401, 106935.

Salaün, A., Villemant, B., Gérard, M., Komorowski, J. C., & Michel, A. (2011). Hydrothermal alteration in andesitic volcanoes: trace element redistribution in active and ancient hydrothermal systems of Guadeloupe (Lesser Antilles). Journal of Geochemical Exploration, 111(3), 59-83.

Siratovich, P. A., Heap, M. J., Villeneuve, M. C., Cole, J. W., & Reuschlé, T. (2014). Physical property relationships of the Rotokawa Andesite, a significant geothermal reservoir rock in the Taupo Volcanic Zone, New Zealand. Geothermal Energy, 2(1), 1-31.

Siratovich, P. A., von Aulock, F. W., Lavallée, Y., Cole, J. W., Kennedy, B. M., & Villeneuve, M. C. (2015). Thermoelastic properties of the Rotokawa Andesite: a geothermal reservoir constraint. Journal of Volcanology and Geothermal Research, 301, 1-13.

Soueid Ahmed, A., Revil, A., Byrdina, S., Coperey, A., Gailler, L., Grobbe, N., ... & Humaida, H. (2018). 3D electrical conductivity tomography of volcanoes. Journal of Volcanology and Geothermal Research, 356, 243-263.

Spieler, O., Kennedy, B., Kueppers, U., Dingwell, D. B., Scheu, B., & Taddeucci, J. (2004). The fragmentation threshold of pyroclastic rocks. Earth and Planetary Science Letters, 226(1-2), 139-148.

Surono, Jousset, P., Pallister, J., Boichu, M., Buongiorno, M. F., Budisantoso, A., Costa, F., ... & Lavigne, F. (2012). The 2010 explosive eruption of Java's Merapi volcano—a '100-year' event. Journal of Volcanology and Geothermal Research, 241, 121-135.

Tang, C. A., Tham, L. G., Wang, S. H., Liu, H., & Li, W. H. (2007). A numerical study of the influence of heterogeneity on the strength characterization of rock under uniaxial tension. Mechanics of Materials, 39(4), 326-339.

Tuğrul, A., & Gürpinar, O. (1997). A proposed weathering classification for basalts and their engineering properties (Turkey). Bulletin of Engineering Geology and the Environment, 55(1), 139-149.

Ulusay, R. (Ed.). (2014). The ISRM suggested methods for rock characterization, testing and monitoring: 2007-2014. Springer.

Ündül, Ö., & Er, S. (2017). Investigating the effects of micro-texture and geo-mechanical properties on the abrasiveness of volcanic rocks. Engineering Geology, 229, 85-94.

van Wyk de Vries, B., Kerle, N., & Petley, D. (2000). Sector collapse forming at Casita volcano, Nicaragua. Geology, 28(2), 167-170.

Villeneuve, M. C., Diederichs, M. S., & Kaiser, P. K. (2012). Effects of grain scale heterogeneity on rock strength and the chipping process. International Journal of Geomechanics, 12(6), 632-647.

Voight, B., Constantine, E. K., Siswowidjoyo, S., & Torley, R. (2000). Historical eruptions of Merapi volcano, central Java, Indonesia, 1768–1998. Journal of Volcanology and Geothermal Research, 100(1-4), 69-138.

Voight, B., Komorowski, J. C., Norton, G. E., Belousov, A., Belousova, M., Boudon, G., ... & Young, S. (2002). The 1997 Boxing Day sector collapse and debris avalanches, Soufrière Hills volcano, Montserrat, WI. The Eruption of Soufriere Hills Volcano, Montserrat, From 1995 to 1999, 363-407.

Watters, R. J., & Delahaut, W. D. (1995). Effect of argillic alteration on rock mass stability. Clay and Shale Slope Instability, 10, 139.

Weaver, J., Eggertsson, G. H., Utley, J. E., Wallace, P. A., Lamur, A., Kendrick, J. E., ... & Lavallée, Y. (2020). Thermal liability of hyaloclastite in the Krafla geothermal reservoir, Iceland: the impact of phyllosilicates on permeability and rock strength. Geofluids, 2020.

Wedekind, W., López-Doncel, R., Dohrmann, R., Kocher, M., & Siegesmund, S. (2013). Weathering of volcanic tuff rocks caused by moisture expansion. Environmental Earth Sciences, 69(4), 1203-1224.

Weydt, L. M., Ramírez-Guzmán, Á. A., Pola, A., Lepillier, B., Kummerow, J., Mandrone, G., ... & Sass, I. (2021). Petrophysical and mechanical rock property database of the Los Humeros and Acoculco geothermal fields (Mexico). Earth System Science Data, 13(2), 571-598.

Wilson, C. J., & Rowland, J. V. (2016). The volcanic, magmatic and tectonic setting of the Taupo Volcanic Zone, New Zealand, reviewed from a geothermal perspective. Geothermics, 59, 168-187.

Wyering, L. D., Villeneuve, M. C., Wallis, I. C., Siratovich, P. A., Kennedy, B. M., Gravley, D. M., & Cant, J. L. (2014). Mechanical and physical properties of hydrothermally altered rocks, Taupo Volcanic Zone, New Zealand. Journal of Volcanology and Geothermal Research, 288, 76-93.

Yasar, S., & Komurlu, E. (2020). Water saturation induced changer in the indirect (Brazilian) tensile strength and the failure mode of some igneous rock materials. Geoscience Engineering, 66, 60-68.

Yavuz, A. B., Kaputoglu, S. A., Çolak, M., & Tanyu, B. F. (2017). Durability assessments of rare green andesites widely used as building stones in Buca (Izmir), Turkey. Environmental earth sciences, 76(5), 211.

Yilmaz, T. I., Wadsworth, F. B., Gilg, H. A., Hess, K. U., Kendrick, J. E., Wallace, P. A., ... & Dingwell, D. B. (2021). Rapid alteration of fractured volcanic conduits beneath Mt Unzen. Bulletin of Volcanology, 83(5), 1-14.

Zhang, Y. (1999). A criterion for the fragmentation of bubbly magma based on brittle failure theory. Nature, 402(6762), 648-650.

Zorn, E. U., Rowe, M. C., Cronin, S. J., Ryan, A. G., Kennedy, L. A., & Russell, J. K. (2018). Influence of porosity and groundmass crystallinity on dome rock strength: a case study from Mt. Taranaki, New Zealand. Bulletin of Volcanology, 80(4), 35.

Xu, T., Fu, T. F., Heap, M. J., Meredith, P. G., Mitchell, T. M., & Baud, P. (2020). Mesoscopic damage and fracturing of heterogeneous brittle rocks based on three-dimensional polycrystalline discrete element method. Rock Mechanics and Rock Engineering, 53(12), 5389-5409.